MAX-PLANCK-INSTITUT
FÜR KOLLOID- UND
GRENZFLÄCHENFORSCHUNG

UNIVERSITÀ DEGLI STUDI DI PADOVA

DIPARTIMENTO DI SCIENZE CHIMICHE
CORSO DI LAUREA MAGISTRALE IN CHIMICA INDUSTRIALE

TESI DI LAUREA MAGISTRALE

In-Situ analyses to investigate photo-catalytic procedures for the formation of Carbon-Oxygen bonds

Relatore: Prof. Fernando Formaggio
Co-relatore: Prof. Bartholomäus Pieber
Controrelatore: Prof. Lorenzo Franco

Laureando: Tommaso Bertolin

ANNO ACCADEMICO 2021/2022

INDEX

RIASSUNTO

Nell'ambito dello sviluppo di nuove reazioni di cross-coupling per ottenere legami carbonio-eteroatomo nei substrati aromatici, i catalizzatori organometallici a base di nichel rappresentano un'alternativa migliore, più economica e più sostenibile rispetto all'attuale stato dell'arte, che prevede l'uso di catalizzatori organometallici a base di palladio.

I catalizzatori organometallici a base di Nickel devono essere accoppiati con dei fotocatalizzatori per favorirne l'eliminazione riduttiva, con la formazione del prodotto e la rigenerazione del catalizzatore iniziale. Tuttavia, in sistemi elettronricchi aromatici si è osservata la degradazione dei catalizzatori a base di nichel con la formazione di nichel metallico inattivo ("Nickel Black"), portando a minori rese e basse conversioni. Attraverso il monitoraggio *in situ* delle reazioni, applicando il "Same Excess Experiment", è stato possibile stabilire l'assenza o meno di tali disattivazioni dei catalizzatori, in 4 sistemi fotocatalitici con organometalli a base di nichel per la formazione di legami C-O, usando substrati aromatici elettron-ricchi.

ABSTRACT

In the context of new cross-coupling reactions developments, to obtain carbon-heteroatom bonds in aromatic substrates, nickel-based organometallic catalysts represent a better, cheaper and more sustainable alternative to the current state of the art, which exploits palladium-based organometallic catalysts.

Nickel-based organometallic catalysts have to be coupled with photocatalysts to promote reductive elimination, with the formation of the product and the regeneration of the initial catalyst. However, in electron-rich aromatic systems, it has been observed the degradation of nickel-based catalysts with the formation of inactive nickel metal ("Nickel Black"), leading to low yields and low conversions. Through *in situ* monitoring of the reactions and applying the "Same Excess Experiment", it was possible to establish the absence or not of such catalyst deactivations in 4 photocatalytic systems with nickel-based organometals for the formation of C-O bonds, using electron-poor aromatic substrates.

INTRODUCTION

The project was conducted entirely at the research laboratory of Doctor Bartholomäus Pieber with the support of his research group at the Max Planck Institute of Potsdam, Germany. The internship was supported by the "Erasmus+ Traineeship" project.

Carbon-carbon and carbon-heteroatom bond forming reactions are key transformations in synthetic organic chemistry, due to the omnipresence of heteroatoms in pharmaceuticals, agrochemicals and natural products.[1-3] A powerful strategy to selectively achieve these bond formations are transition metal-catalyzed cross-coupling reactions.[4] Various traditionally used C-C and C-Het cross-coupling reactions are based on rare palladium catalysts, rendering these reactions unsustainable and uneconomical in the long-term use.[5-7] Due to its ability to catalyze many of the same reactions, nickel was found to be a dignified replacement for palladium.[8] The significantly lower reduction potential of nickel has major drawbacks, despite the mechanistic similarities to Pd-catalyzed reactions.[9] To exploit a metal in cross-coupling reactions, its catalytic cycle must be continuous and have rapid kinetics. A promising strategy for making the catalytic steps equally fast is photocatalysis.

Photocatalysis is a field of research that has evolved rapidly over the last century. It expands the opportunities of synthetic organic chemistry, thanks to the benefits from the economic and ecological advantages to exploit the freely available natural sunlight.[10-11] There are two main differences between photocatalysis and traditional catalysis. Photocatalysts accelerate the reactions by increasing the potential energy of the reactants and/or intermediate compounds facilitating the overcoming of the energy barrier.[12] Conversely, traditional catalysts decrease the energy of the transition state, by acting directly on the structure of the activated complex.[13]

Nickel, during these processes, goes through catalytic cycles which are not fully known, passing through different oxidation states relating to Ni(I) and Ni(III).[14-15] The current mechanistic hypothesis for the Nickel catalysts depends on the nature of the applied photocatalyst. In the aryl-amination, using $Ir(ppy)_3$ as a photocatalyst, the cycle begins with the reduction of the $NiCl_2$ glyme (**A**) species to an active species (Figure 1). The active species starts the oxidative addition of aryl halide (**B**) to Nickel complex (**C**) forming an intermediate complex (**D**), which undergoes a ligand exchange with a nucleophile (**E**) that releases a halide anion (**F**) and generates the intermediate complex (**G**). Upon irradiation, the photocatalyst harvests energy from the photons, to achieve an electronically excited state. The subsequent step provides an EnT

by the excited photocatalyst **(PC*)**, that triggers the reductive elimination thus forming the cross-coupled product (**I**) and regenerating the Nickel complex (**C**) (Figure 1).[16]

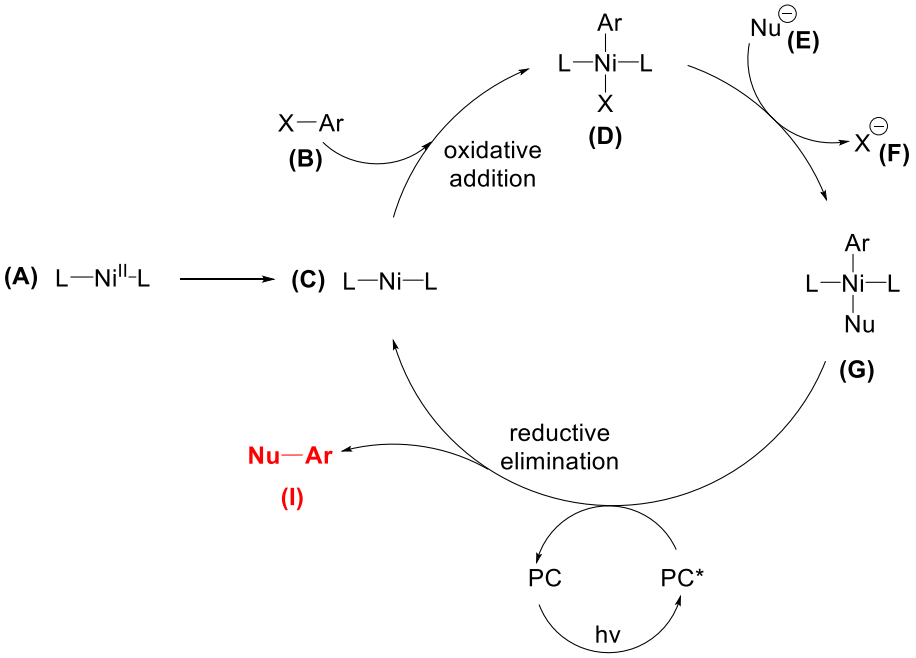

Figure 1: Proposed Mechanism for Nickel-based cross-coupling reaction[16]

Photocatalysts are all the compounds which can collect light energy and exploit it, to produce chemical transformations in other reagents and regenerating their chemical structures after each cycle.[17] There are several compounds used as photocatalysts, all of which share the common ability to absorb visible light energy through electronic transition. The collected energy is transferred to the reagents via photoredox mechanisms or energy transfer mechanisms.[18] There are many compounds applicable as photocatalysts, which can be divided into two categories: homogeneous photocatalysts and heterogeneous photocatalysts.[19] The commonly used homogeneous photocatalysts are metalorganic compounds transition metal bipyridine complexes, such as Ir or Ru. These homogeneous photocatalysts were used by MacMillan in reactions for cross-coupling with nickel.[16] However, these metalorganic compounds are not cheaply available, and because they are homogeneous, such catalysts need to be removed from the reaction mixture at the end of the process, requiring possible purification steps and not allowing an easy way to recycle them. This has led to the research of recyclable solid materials that can be applied as photocatalysts.

Pieber and coworkers have developed several procedures in the last three years in which cheaper photocatalysts have replaced the expensive Iridium-based photocatalysts.[20-23] Among these compounds,

semiconductors of the carbon nitride class are particularly efficient, recyclable, thermostable, and cheap.[20-21] Non exogenous photocatalyst nickel-complexes were developed as the next generation systems. The energy required for nickel turnover can be absorbed through the chromophore groups of certain organometals, where nickel is directly bonded to functionalized bipyridine ligands .[24]

Although the possibility of replacing the use of palladium in cross-coupling reactions, with dual-nickel and photocatalytic systems, is particularly promising, these techniques rely on cycles of oxidative addition and reductive elimination, whose rates are not equal, especially for electron-rich substrates. These mechanisms rely on the initial reduction of the Ni(II) species to Ni(I) or Ni(0); from these low valent species the oxidative addition is slow for electron-rich aromatic substrates.[25] A consequence of applying photocatalysts, to enable the thermodynamically unflavored reductive elimination, is that it can lead to the aggregation of low-valent nickel species.[26] It was demonstrated by Pieber and coworkers, in nickel-catalyzed cross-coupling amination involving electron-rich aromatic substrates, that low-valent nickel species can coagulate to nickel metal nanoparticles, known as "nickel black", leading to catalyst deactivation. This happens when the oxidative addition rate is lower than the reductive elimination rate.[26] These results call for further studies to investigate whether catalytic deactivation is also present with other types of substrate.

2. AIM OF THE PROJECT

This project aimed to investigate whether catalytic deactivation or product inhibition is present when the Nickel-complex catalysts for cross-coupling are coupled with photocatalytic C-O cross-coupling systems. An elegant way to obtain this information is by applying *in situ* monitoring, an important tool available for obtaining rapid and unambiguous information on the kinetics of the reaction concerned. Information is collected on the progress of the reaction over time, through the online visual analysis of the developments in the concentration of reagents, products, and intermediate species. These techniques are non-destructive analyses, and do not require sample preparation. In addition, they give a large amount of useful data from the reaction system that is not disturbed by the analyses itself. For these last reasons the *in situ* monitoring methods are applied for reaction progress kinetic analyses.

These techniques, along with the FTIR emission spectroscopic analysis, will be applied to the "Same Excess Experiment" to determine the slopes of reagents and products during the reaction time.

We will investigate the robustness of 4 different photocatalytic systems with optimized procedures, using as model an esterification between an electron-poor aromatic halide, 4-methyl-iodobenzoate (Ar-I) (**1**) or 4-methyl-bromobenzoate (Ar-Br) (**10**), and the nucleophile *N*-tert-Butoxycarbonyl-*L*-proline (*N*-Boc-Pro-OH) (**2**), under strong irradiation at 440 nm to produce 1-(tert-butyl) 2-(4-methoxycarbonyl)phenyl)pyrrolidine-1,2-dicarboxylate (Prod) (**3**) (Figure 2). Electron-poor species will be used as substrate to verify if they are responsible for possible catalyst deactivation, as shown with similar substrates in cross-coupling amination.[16, 26]

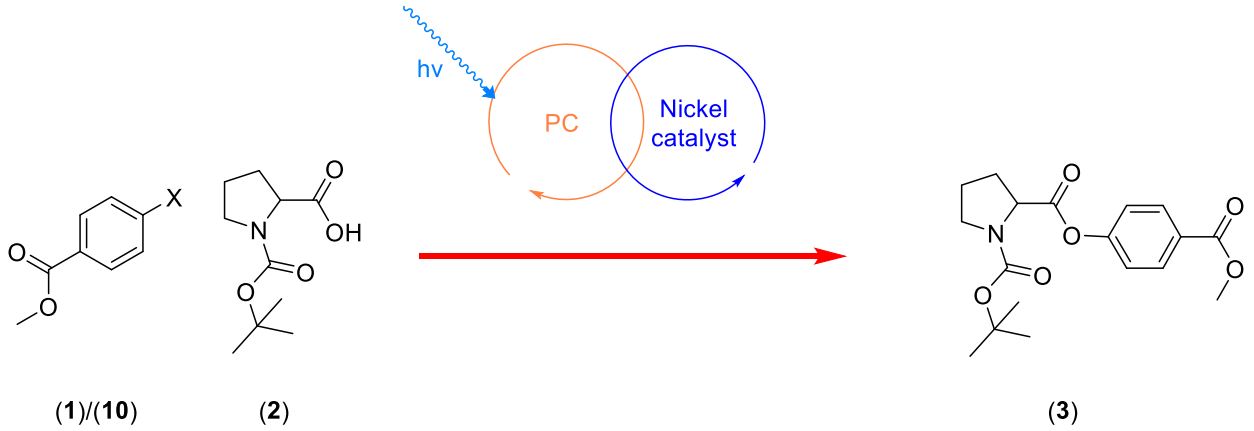

Figure 2 General representation of Cross-coupling reaction photo-nickel catalyzed

3. CATALYTIC SYSTEMS EMPLOYED IN THIS WORK

3.1 HOMOGENOUS DUAL-PHOTOCATALYTIC SYSTEM $Ir(ppy)_3$ –Nickel(II):

The catalytic system consists by the coupling of two homogenous compounds, the nickel complex (**5**) generated by the coupling between the 4,4'-di-*tert*-butyl-2,2'-bipyridine (dtbbpy) and the Nickel(II) bromide diethylene glycol dimethyl ether complex (NiBr2diglyme) as catalyst, and the Tris(2-phenylpyridine)iridium ($Ir(ppy)_3$) (**3**) as photocatalyst (Figure 3). All the compounds are commercially available.[8]

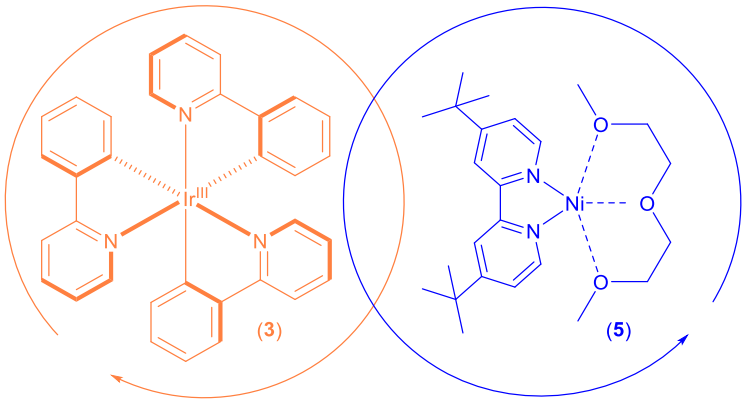

Figure 3: Representation of the photocatalytic system $Ir(ppy)_3$-Nickel(II)[8]

3.2 SEMI-HETEROGENEOUS DUAL-PHOTOCATALYTIC SYSTEM g-CN-OA-m – Nickel(II):

The catalytic system consists in the coupling with solid graphitic carbon nitride (g-CN-OA-m) (**6**) as photocatalyst, easily synthesizable from a commercially available precursor, and as catalyst the Nickel complex (**7**), generated by the coupling between the 4,4'-di-*tert*-butyl-2,2'-bipyridine (dtbbpy) and the Nickel(II) chloride ethylene glycol dimethyl ether complex ($NiCl_2$glyme) (Figure 4).[20]

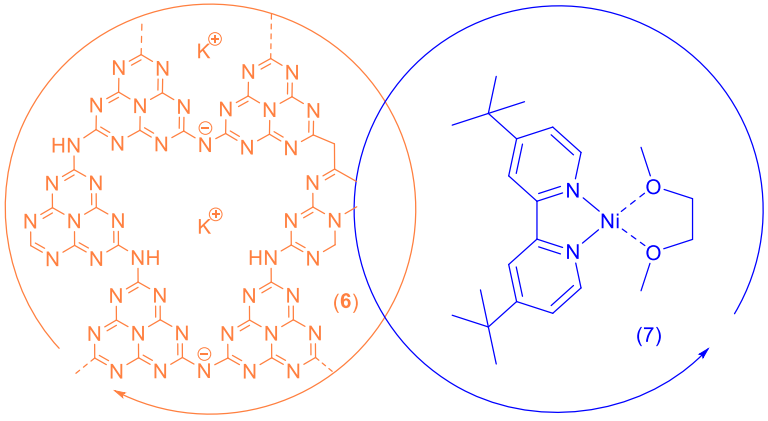

Figure 4: Representation of the photocatalytic system g-CN-OA-m – Nickel(II)[20]

3.3 HOMOGENOUS SINGLE-PHOTOCATALYTIC SYSTEM Ni(II)-czbpy:

The photocatalytic system consists of the homogenous Nickel complex (Ni(II)-czbpy) (**8**) obtained by the coupling with the ligand 5,5'-di(9*H*-carbazol-9-yl)-2,2'-bipyridine (czbpy) and the Nickel(II) chloride ethylene glycol dimethyl ether complex (Figure 5). The ligands were previously synthesized.[24]

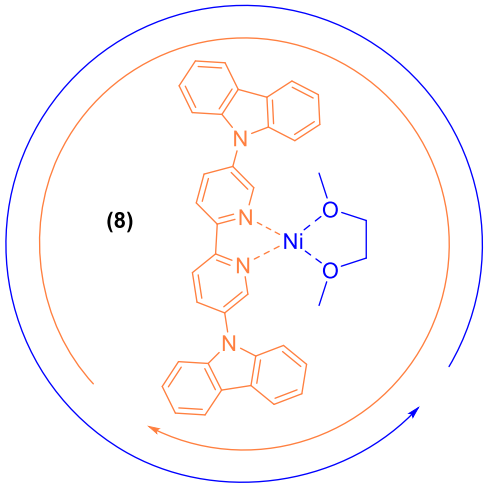

Figure 5: Representation of the photocatalytic system Ni(II)-czbpy[24]

3.4 HETEROGENEOUS SINGLE-PHOTOCATALYTIC SYSTEM poly-Ni(II)-czbpy:

The photocatalytic system is an heterogeneous porous polymer, it consists of a Nickel complex (Ni-czbpy) (**9**) obtained by the coupling with the ligand poly-5,5'-di(9H-carbazol-9-yl)-2,2'-bipyridine and the Nickel(II) chloride ethylene glycol dimethyl ether complex (Figure 6). The ligand was previously synthesized and polymerized.[24]

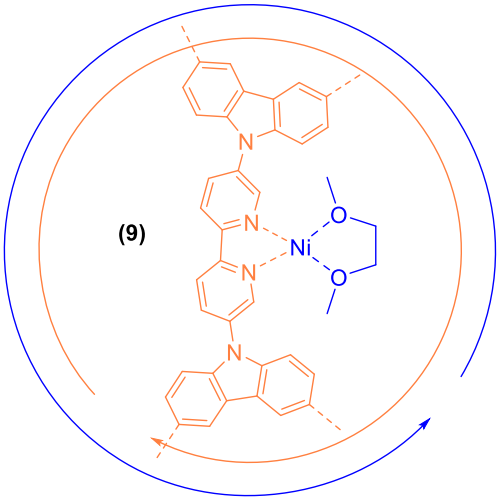

Figure 6: Representation of the photocatalytic system poly-Ni(II)-czbpy[24]

4. THEORETICAL BACKGROUND

4.1 KINETIC INVESTIGATIONS THROUGH SAME EXCESS EXPERIMENT

The Same Excess Experiment procedure is a Visual Time Normalization Analysis (VTNA), which exploits the concentration-against-time reaction profiles to obtain kinetic information. It consists of initially conducting two experiments of the same reaction, in the same conditions, but with different reagent concentrations, maintaining an initial equal excess between them in both experiments. During the reaction time, it is necessary to choose and measure extensive properties, which can be quickly converted into concentration profiles of the reactants and products. For this reason, it is proposed to collect *in situ* spectroscopic absorbance data of the compounds involved in the reaction.

The consumption of a reagent can be described by a generic mathematical function, depending on the mechanism of the reaction itself.[27] The normalized excess between the reagents in the reaction is constant during the whole reaction time. Therefore, the reaction started at lower concentrations can be considered as the reaction at higher concentrations, after it has consumed part of its reactants. In both situations the molar excess is the same.[28]

Table 1: Example of reaction studied for Same Excess Experiments with below the conditions for the excess

$$mA + nB \rightarrow pC$$

$$e = \frac{[A]_0}{m} + \frac{[B]_0}{n}$$

	[A]	[B]	e
Initial concentration	$[A]_0$	$[B]_0$	$\frac{[A]_0}{m} + \frac{[B]_0}{n}$
Concentration at instant t	$[A]_t$	$[B]_t$	$\frac{[A]_0}{m} + \frac{[B]_0}{n}$

This condition is maintained even if there are phenomena which can vary the reaction rate during the process.[29] The two phenomena of product inhibition and catalyst deactivation, if present, slow down the rate of consumption of the substrate. This means that the functions describing the substrate consumption in the two reactions have different slope. This is because the reaction at higher initial concentrations slows down before, during, and after it reaches the initial concentration of the second reaction, decreasing

slowly. The difference between the two slopes is visualized after shifting to the right the second reaction, until its maximum value reaches the corresponding value of the first reaction (Figure 7).

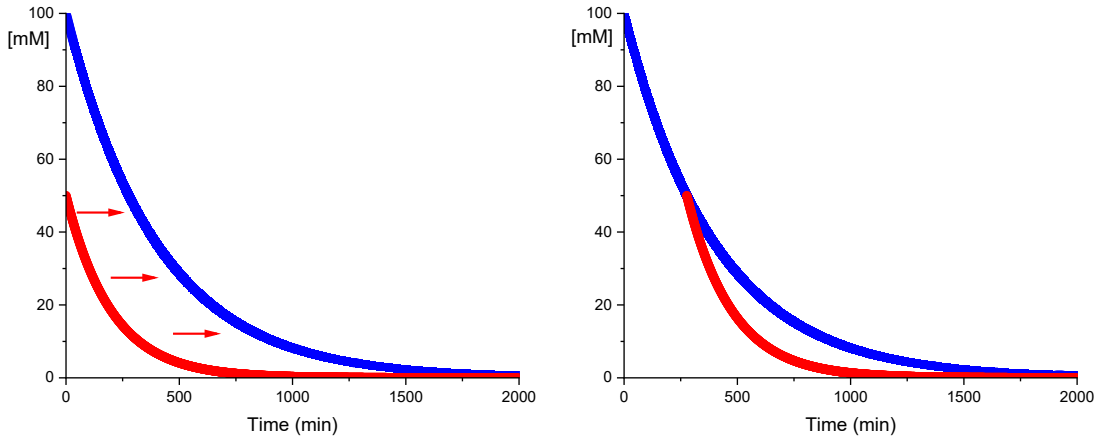

Figure 7: Presence of catalyst deactivation or product inhibition

To discriminate between the possibility of catalyst deactivation or product inhibition, it is necessary to carry out a third experiment. In this case, concentrations are those of the reaction with lower initial concentrations, but it is added to the mixture an amount of the product that would have been formed in the reaction at higher initial concentrations, when the latter has reached the same initial concentration of reactants as the reaction at lower concentrations. The third reaction is identical to the reaction at lower initial concentrations, except for the number of turnovers performed by the catalyst. If the presence of the product reduces the reaction rate of the process, then there will be an overlap between the functions describing the consumptions of reagents.

If there is no-overlap between the reaction progress profiles, describing reagent consumption, it means that there is not the same amount of catalytic turnovers during the third experiment and in the reactions at lower initial concentrations. This indicates that the catalyst is deactivated during the process (Figure 8).[28, 30]

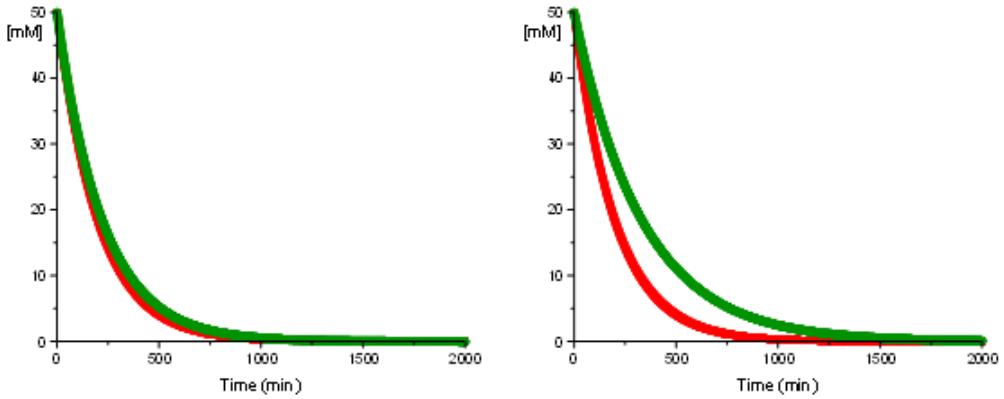

Figure 8: Product inhibition (left) and catalyst deactivation (right)

The main advantage of Same-Excess Experiment is that it can provide direct information from the simple observation of concentration plots, which are obtained by basic mathematical operations of proportions from absorbance datasets.

4.2 PHOTOCATALYSIS AND NICKEL COMPLEXES

The field of photocatalysis concerns reactions promoted by light energy and light absorbing species.[17] Upon excitation with visible light, the photocatalyst can access electronic excited states. The excited state energy is transferred to a second species, triggering a chemical reaction.[12] These processes can take place via two possible mechanisms, through energy transfer catalysis or photoredox catalysis.[18]

The combination of a Nickel complex cycle and the photocatalyst cycle in the cross-coupling reaction relies both on the mode of activation of the photocatalyst and on how it interacts with the substrate. The following sections describe the physical processes by which photocatalysts release energy to the substrate, along with the catalytic cycles through which C-O bonds are formed.

4.2.1 PHOTOREDOX MECHANISM

In photoredox catalysis, quenching of the photoexcited species can occur via single electron transfer (SET) mechanisms. Upon UV-visible light irradiation of the photocatalyst (PC) a ground state electron gets promoted to an excited state and undergoes intersystem crossing (ISC), resulting in a long-lived triplet photo-excited state (PC*). Due to the consequently formed vacancy in the respective ground state orbital, the excited photocatalyst can act as a reductant agent or as an oxidant agent. At this point the reduced, or the oxidized photocatalyst, goes through a second electron transfer with either a reducing or an oxidizing support agent, regenerates the original photocatalyst (PC) (Figure 9). [31-32]

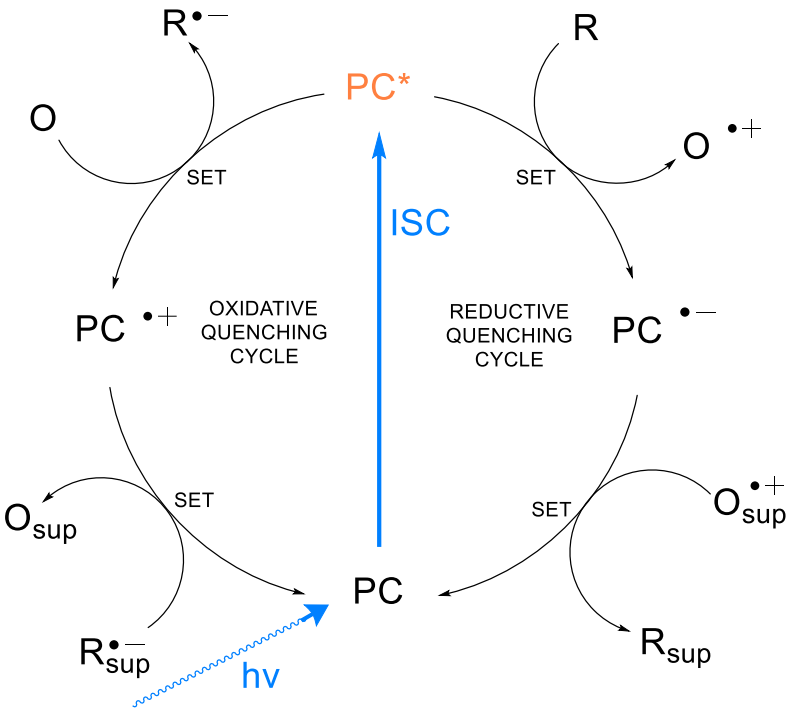

Figure 9: Reductive and oxidative quenching cycles

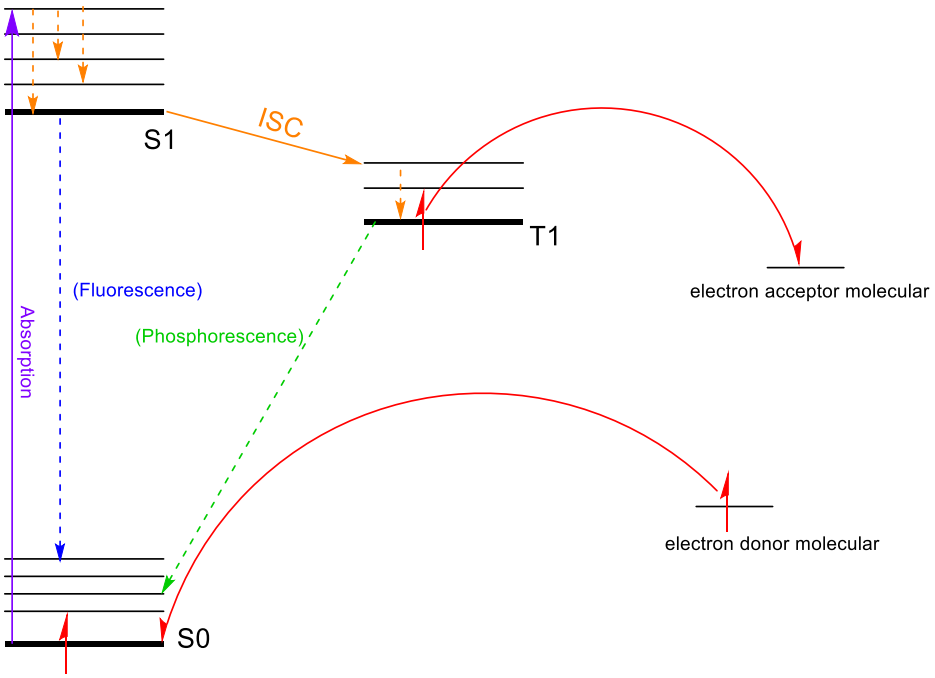

Figure 10: Jablonski diagram of the photocatalyst during the photoredox mechanism

The photoredox mechanisms for the photocatalysts $Ir(ppy)_3$ and g-CN-OA-m are explained in the next sections.

4.2.1.1 PHOTOREDOX MECHANISM PROPOSED FOR $Ir(ppy)_3$

The $Ir(ppy)_3$ photocatalyst can undergo, through irradiation with blue light, a charge transfer from metal to ligand (MLCT) and subsequently goes through intersystem crossing (ISC) (Fig. 11). These two consequent events bring an electron into an excited triplet state in an empty π orbital with a lifetime of 1.9 μs. The excited complex can act as oxidizing agent. The reduced $Ir(ppy)_3$ catalyst, subsequently undergoes a second electron transfer event, this time acting as a reducing agent, returning to the initial situation (Figure 11).[33]

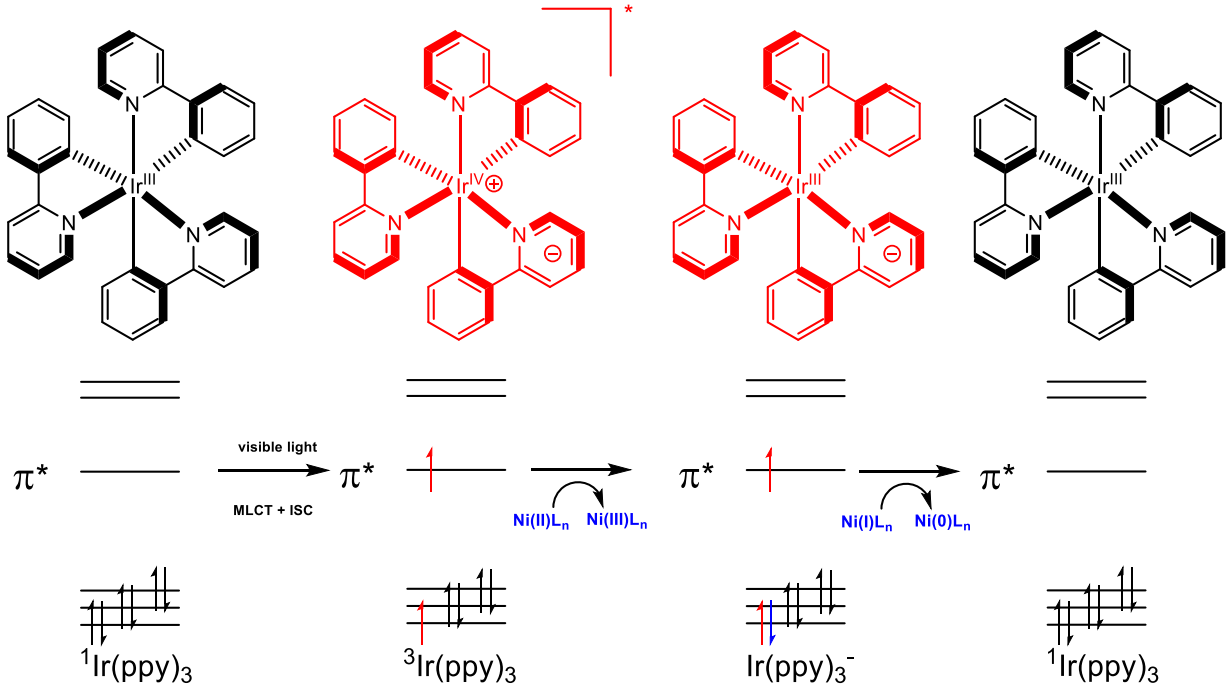

Figure 11

Nocera and coworkers propose a possible mechanism in nickel catalyzed cross-coupling reaction (Figure 12).[15] This thesis is obtained by the study of the etherification between aryl halides and methanol, which is involved in a Ni(I)/Ni(III) catalytic cycle, where a precatalytic cycle is present and it governs the catalytic action. According to this model, the Ni(II) species (**A**) is reduced by the action of the photocatalyst to a Ni(I) species (**B**), which dimerizes (**C**) with the excess Ni(II) (**A**) present in the system, coordinating it with the amine support base. The dissociation of the dimer (**C**) is essential for the continuation of the reaction, after which the Ni(I) species undergoes an oxidative addition with the aromatic halide (**D**), and it is oxidized to Ni(III) species (**E**) by carrying out the ligand change with the nucleophile (**F**). The oxidized Ni(III) new complex (**G)** is energetically favored to carry out the reductive elimination, thus producing the new carbon-oxygen bond compound (**H**) and regenerating the Ni(I) catalyst (**B**).[15] The photocatalytic redox

cycle is closed by the reduction of the cationic species, probably by the amine, through a single electron transfer (Figure 12).[15, 34]

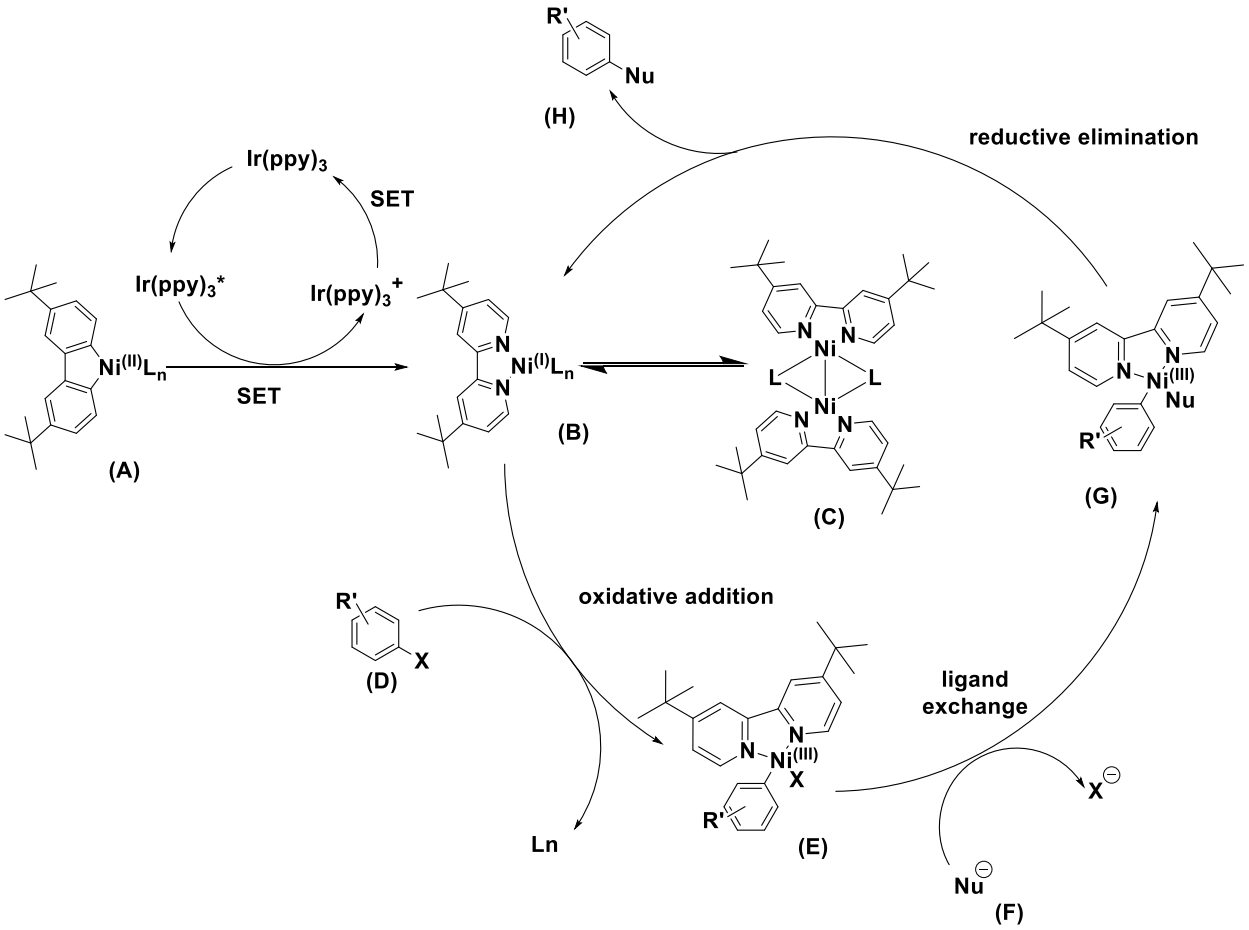

Figure 12: Catalytic cycle proposed for the photoredox mechanism in presence of $Ir(ppy)_3$

4.2.1.2 PHOTOREDOX MECHANISM PROPOSED FOR g-CN-OA-m

The carbon nitrides are metal-free semiconductors, easily synthesizable from cheap materials containing carbon and nitrogen, such as oxamide and urea. They absorb light in the near UV and the visible region, depending on factors related to stoichiometry and the preparations of the polymer. They can also endure high temperatures in very harsh conditions, maintaining flexible structures. The g-CN materials have a bandgap close to 2.7 eV (blue region), which can be tuned by factors such as the C/N ratio, the polymerization degree, and the morphological texture of the structures.[35]

Pieber and coworkers developed a semi-heterogeneous methodology for the cross-coupling carbon-oxygen bond, using as photocatalyst the mesoporous semiconductor g-CN-OA-m. The surface sites of the graphitic carbon nitrides can bond with ligand atoms, giving them an interesting feature for reactions

involving electronegative atoms.[20] This particular material shows a higher absorbing capability than the Iridium photocatalysts, around 400 nm and 480 nm, thanks to the electronic transitions π-π* of the double bonds C=N and n-π* of the free pairs of nitrogen atoms.[36]

The formation of carbon-heteroatom bonds can be catalyzed using, as photocatalytic agents, solid semiconductors substances, which can absorb light, to promote an electron from the valence band (VB) to the conduction band (CB). This generates, in the same species, a possible oxidant or reductant agent. The electron holes (h+) can act as a reductant agent via oxidation itself, while the excess electrons (e-) act as an oxidant agent via reduction itself. Both mechanisms happen through single-electron transfer. After the SET, the process is undergone again to regenerate the original configuration of the semiconductor (Figure 13).[37]

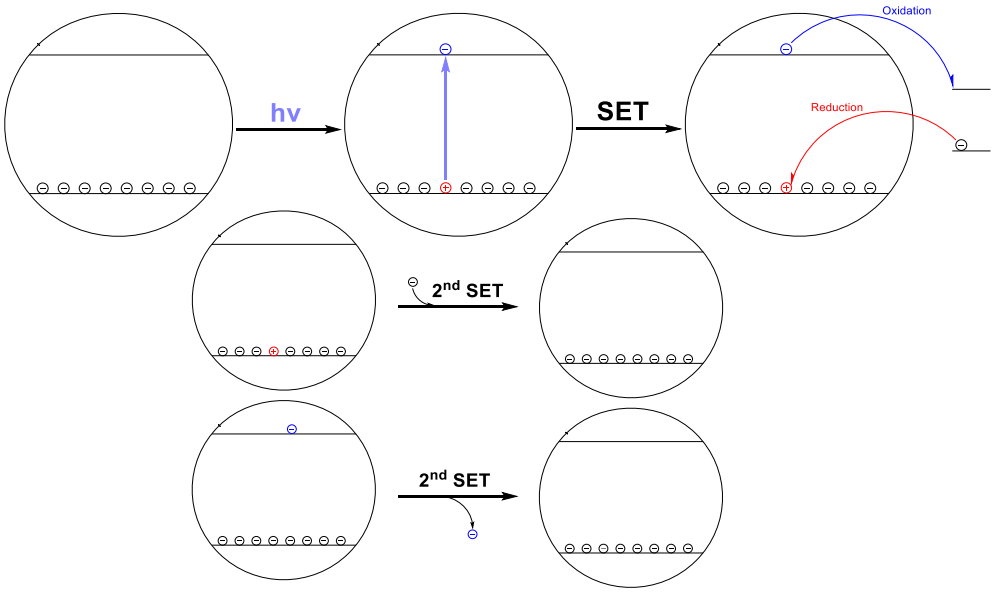

Figure 13 SET mechanism for semiconductor

The mechanism (Figure 14) proposes that there are two electron transfer interventions, one to the nickel catalytic cycle, and the other being the reduction of the substrate by the photocatalyst which promotes oxidative addition.[34] The mechanism begins with the reduction of the Ni(II) precatalyst (**A)** to Ni(I) or Ni(0) species (**B**), as suggested by Nocera and coworkers.[15] In this thesis, it is suggested that the photocatalyst, when it is in the photoexcited energy state (a necessary condition) (**PC***), acts as a reducing agent to form a radical anion (**D**) on the aromatic substrate (**C**), and as a consequence, the cationic photocatalytic compound (**PC**$^{+}$). After that there is the oxidative addition, resulting in the formation of complex (**E**),

followed by that, the ligand exchange with the nucleophile (**F)** produces the complex (**G**). This complex undergoes an excitation with the excited photocatalyst (**PC***), which gives the reactive species (**H**) the necessary energy to complete the reductive elimination generating the final product (**I**). This process would occur for both homogeneous and heterogeneous catalysts and would be supported by the fact that aryl bromides are converted in smaller quantities, when photocatalysts with lower reduction potentials are used. This is demonstrated by kinetic laws, when the system is irradiated by an unlimited number of photons. In the case of using a homogeneous catalyst such as $Ir(ppy)_3$, which has a reduction potential of -1.73 V vs. SCE, there is no dependence on the concentration of the aromatic substrate, but only on the concentration of the nickel complex.[34] On the other hand, the kinetic law for the process with the g-CN-OA-m catalyst presents a dependence with a fractional exponent of 0.3 for the aromatic substrate. This suggests there is an unfavorable phenomenon concerning this compound, which can be assumed to be the reduction of the substrate itself by the catalyst, which possesses a reduction potential of -1.65 V vs SCE.[34]

This mechanism, therefore, proves that there may be possible limiting events during the entire process. In the case of homogeneous iridium-based catalysts with lower reduction potentials, the reductive elimination step is very fast, which should not give the catalyst the time to recover in its own cycle. On the same principle, this would be the case with heterogeneous catalysts with higher reduction potentials, for which the reduction of the aromatic substrate can take place with slower kinetics.[34]

The radical anion (**D**) then undergoes an oxidative addition with the nickel complex (**B**), which in turn proceeds in a ligand exchange with the nucleophile (**F**), resulting in the intermediate (**G**) before the reductive elimination action. Before the reduction, there is energetic excitation by the photocatalyst, which excites or oxidizes the nickel complex (**H**), resulting in the formation of the product (**I**) (Figure 14). This model would also explain the role of the additive base, which could be the reducing agent for the oxidized photocatalysts needed to restore it.[34]

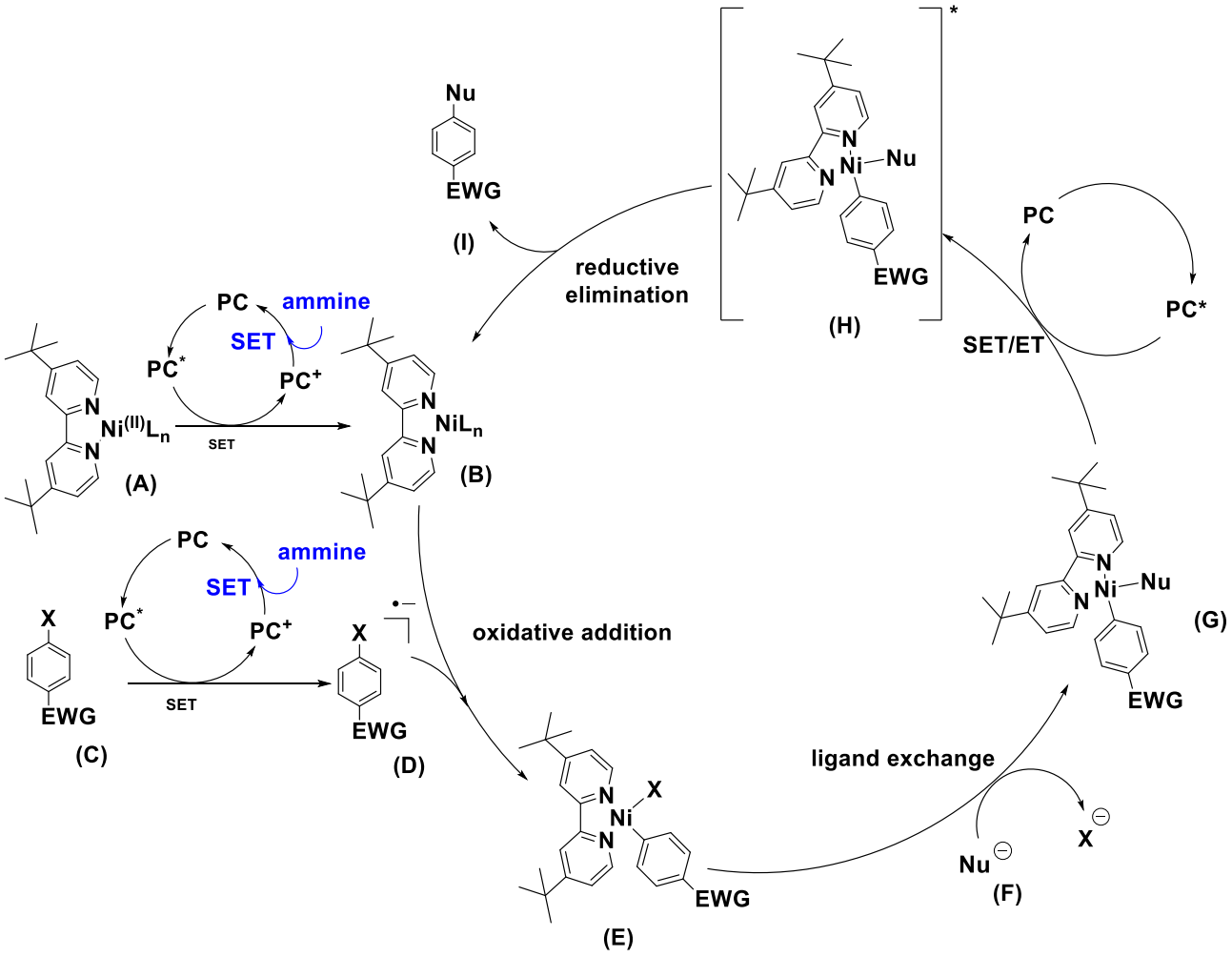

Figure 14 Catalytic cycle proposed for the photoredox mechanism in presence of the g-CN-OA-m

4.2.2 ENERGY TRANSFER MECHANISM

Energy transfer (EnT) is a process in which a photo excited molecule (donor*) is quenched by another molecule (acceptor) in a non-radiative event. The donor-acceptor interaction can proceed through two different pathways, giving the same results.[38] Förster Resonance Energy Transfer (FRET) is the mechanism where the donor* transfers the excited state energy via dipole-dipole coupling, to a nearby chromophore. The energy released during the LUMO-to-HOMO transition in the donor excites an electron in the acceptors HOMO (Figure 15). Due to the electrostatic nature of the mechanism, an overlap between the fluorescence emission spectra of the donor and the absorption spectra of the acceptor is required, it has a range from 10 to 100 Å (Figure 16).[39]

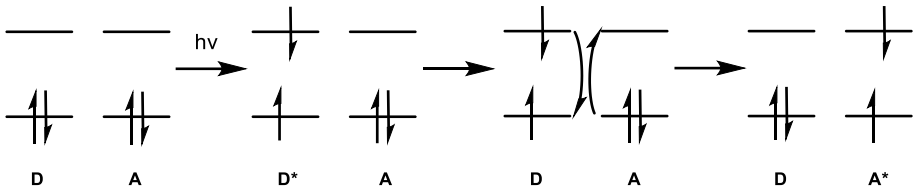

Figure 15: Forster Resonance Energy Transfer (FRET) interactions between donor excited and acceptor

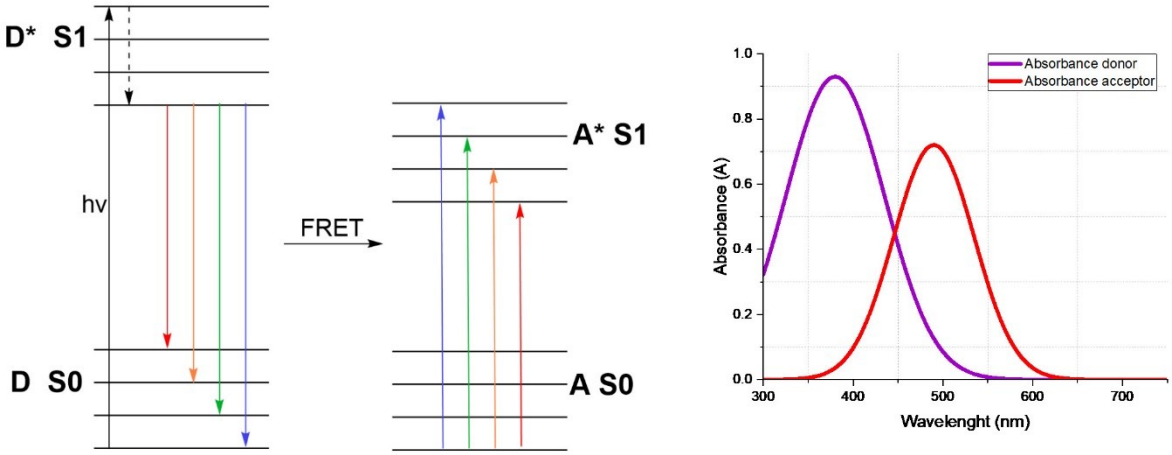

Figure 16 Representation between the fluorescence emission spectra of the donor and the absorption spectra of the acceptor

Dexter energy transfer involves the intermolecular exchange of an excited state electron from the donor with a ground state electron to the acceptor molecule. The donor and acceptor form a collision complex, resulting in an orbital overlap, which enables the exchange of the respective electrons (Figure 17).[40]

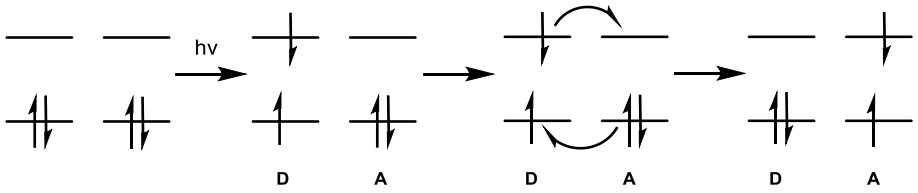

Figure 17 Double-electron exchange between excited donor and acceptor in Dexter energy transfer mechanism

4.2.2.1 ENERGY TRANSFER MECHANISM PROPOSED FOR $Ir(ppy)_3$

The photocatalyst species $Ir(ppy)_3$ can undergo a Dexter energy transfer in the cross-coupling between aryl halides and heteroatoms. The $Ir(ppy)_3$ singlet state is excited to the active triplet state through a MLCT and ISC, which returns to the singlet state after the energy transfer (Figure 18). The Dexter mechanism is more probable in the studied cross-coupling reactions, because there is not enough overlap between the emission spectra of $Ir(ppy)_3$ and nickel complexes.[8]

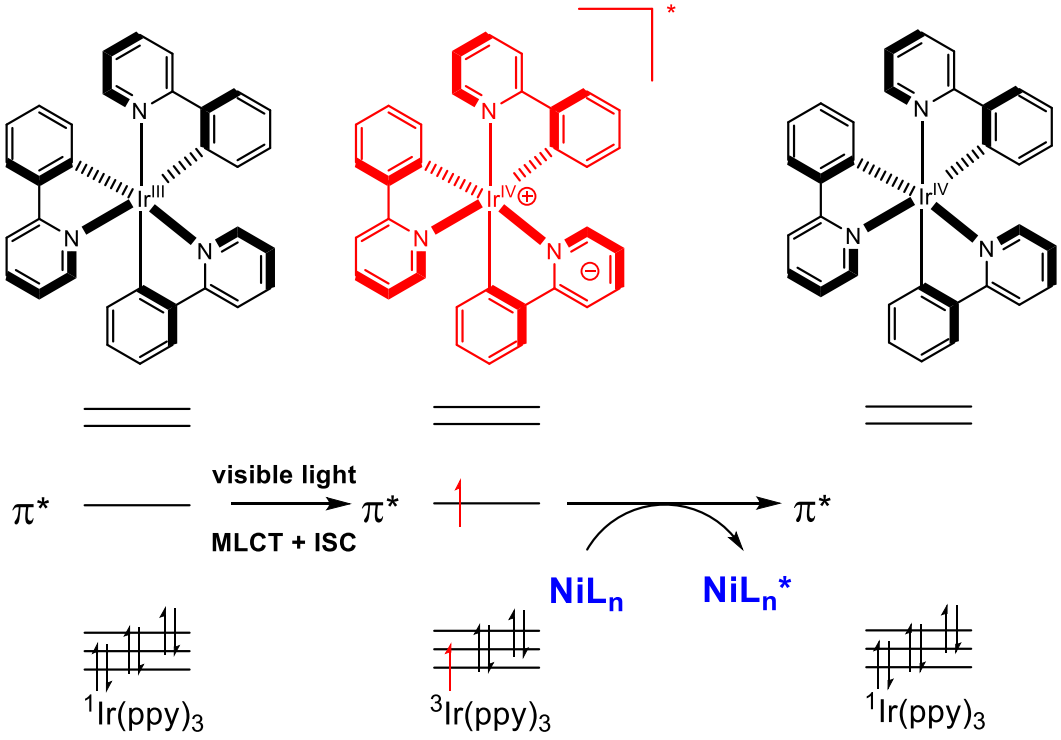

Figure 18 Energy Transfer mechanism between the triplet state Ir(ppy)$_3$ and the Nickel ligand

The proposed catalytic cycle starts with the reduction of the Nickel (II) (**A**) species; there is the reduction of Nickel (0) species (**B**), by electron transfers caused by the photocatalyst. Then the cycle begins with the oxidative addition of aryl halide (**C**) to the Ni(0) complex, followed by a ligand exchange halide-oxygen nucleophile. The new Ni(II) (**D**) complex receives energy from the excited Iridium-based photocatalyst (**PC***), leading to a favorable eliminative reduction from the excited complex (**E**) and the formation of the new carbon-oxygen bond species (**F**). Meanwhile, the reduced Nickel (0) complex (**B**) starts a new catalytic cycle with the aryl halide (Figure 19).[8]

The energy transfer is more probable than an electron transfer, because as the photocatalyst reduction potential decreases, the yield decreases as well, disproving a photoredox mechanism.[8]

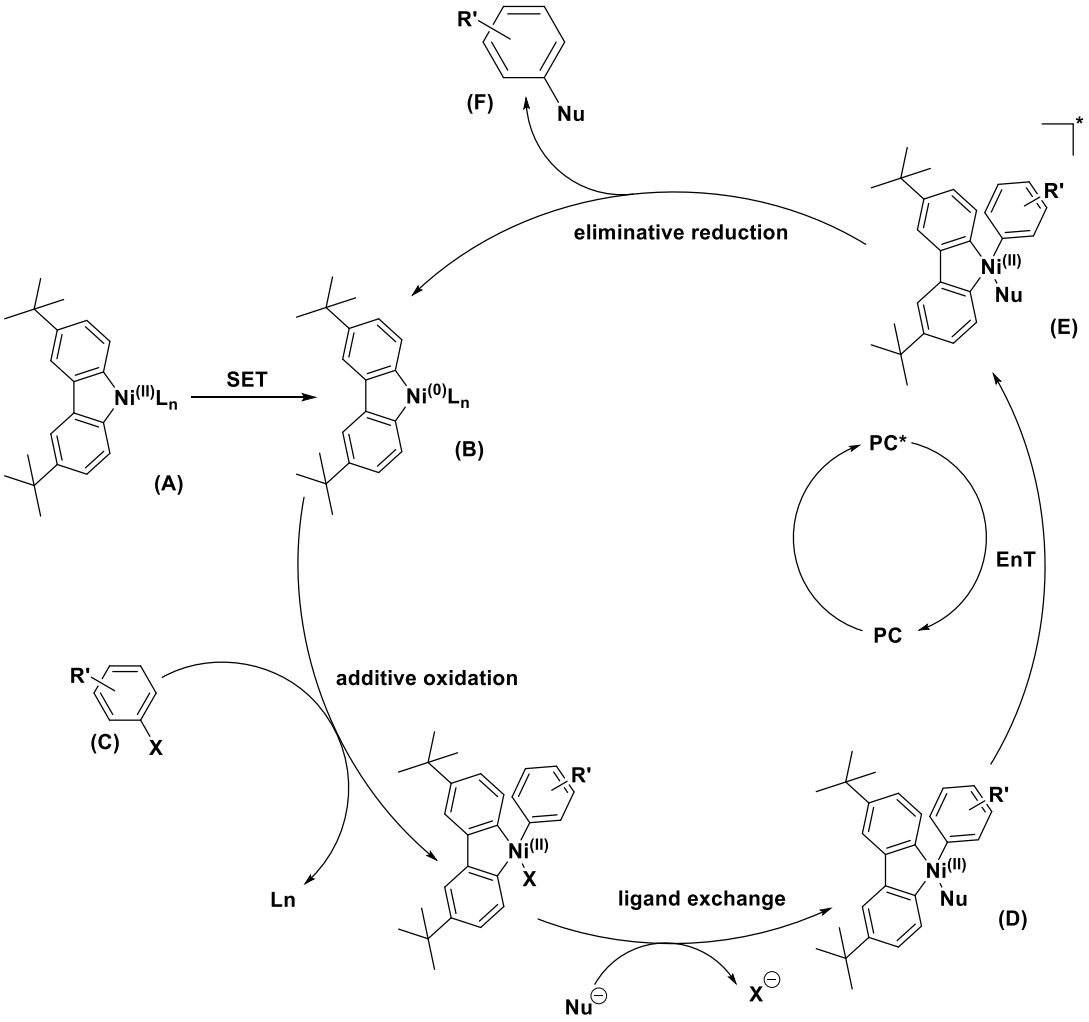

Figure 19 Catalytic cycle proposed for energy transfer mechanism in presence of $Ir(ppy)_3$

4.2.2.2 ENERGY TRANSFER MECHANISM PROPOSED FOR g-CN-OA-m

The indications of the mechanism suggest that there are not reactions involving electronic transfer, but rather energy transfer processes.[20]

4.2.3 UNDETERMINED MECHANISM FOR SINGLE PHOTOCATALYTIC SYSTEMS Ni-czbpy AND poly-Ni-czbpy

Pieber and coworkers developed a new type of catalysts that requires neither noble metals nor other typologies of second photocatalysts. It is a nickel complex (Ni-czbpy) bound to a functionalized bipyridine ligand with two chromophore carbazole groups, acting as antennae to collect energy from visible light.[24] The mechanism relies on intramolecular energy transfer or an intramolecular electron transfer between the ligand and the nickel core. This reduces the metal center from a Ni(II) species (**A**) to a Ni(I) species (**B**),

leading to an active site for the oxidative addition with an aryl halide (**C**). After the oxidative addition, the Ni(III) oxidized complex (**D**) easily undergoes ligand exchange with a nucleophile (**E**) to obtain the complex (**F**). Following this, reductive elimination occurs producing the desired product (**G**) and regenerating the initial Ni(I) complex (**B**) (Figure 20).[24]

From the development of this new catalyst, it has been extended the scope to adapt this photocatalyst-free approach in a heterogeneous reusable system, through the polymerization of the czbpy ligand, has been expended. The result is a microporous polymer (poly-Ni(II)-czbpy), obtained through an oxidative polymerization with iron (III) chloride. SEM analysis confirms that the polymer can bind the nickel complex on its surface homogeneously. The reported spectroscopic data shows that the polymer bonded to the Nickel (II) complexes have the same maximum absorption peak at 450 nm. Thus indicating that the energy levels of the chromophore have not been changed by the polymerization, and can also be utilized to withdraw energy from visible light.[24]

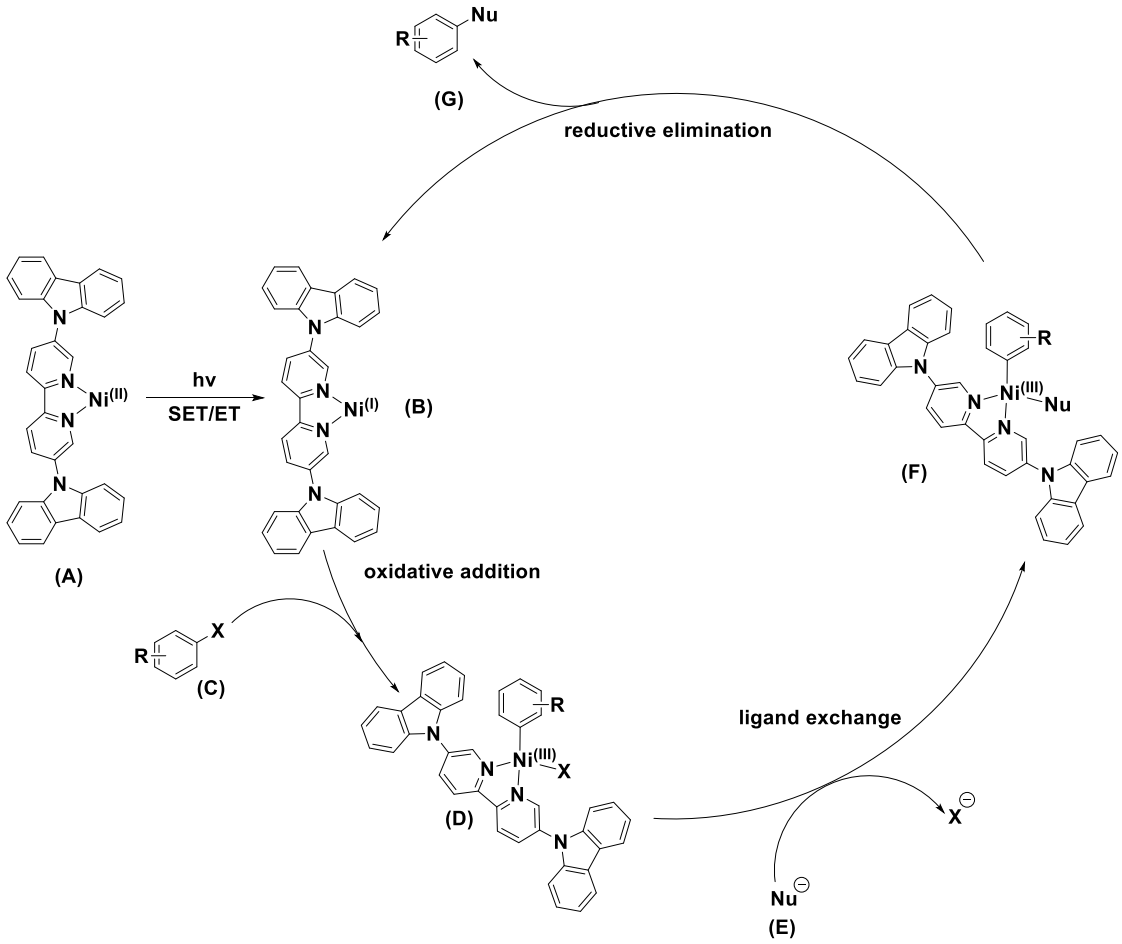

Figure 20 Catalytic cycle theorized for coupled Ni-Czbpy and poly-Ni-Czbpy systems

5. RESULTS AND DISCUSSIONS

In this work we investigated the four photocatalytic systems described in chapter 2 (Aim of the project) using the Same Excess Experiment procedure. For all four catalytic systems, the same esterification reaction was studied, repeated twice, at lower concentrations of reagent and at higher concentrations of reagent. The procedure of the Same Excess Experiment requires to have the concentrations of the photocatalytic compounds in the same relative proportions in both experiments, at low and high concentrations. The amounts of the photocatalytic compounds must be maintained in reactions at lower concentrations. The electron-poor aromatic substrates 4-methyl-iodobenzoate (Ar-I) (**1**) or 4-methyl-bromobenzoate (Ar-Br) (**10**) were used as reference reagents. The nucleophile used in this project was N-tert-Butoxycarbonyl-L-proline (N-Boc-Prol) (**2**). The same conditions were required in all the procedures, with anhydrous DMSO as a solvent, *N*-isopropyl-2-methylpropan-2-amine (BIPA) (**11**) as a base, under strong blue irradiation at 440 nm and at room temperature, as suggested by the respective optimized procedures (Figure 21).[8, 20, 24] Each reaction was conducted while the infrared emission spectrum of reaction mixture was collected.

The same 50 mM difference between the nucleophile and the substrates was maintained for all reaction pairs. Reaction mixtures at higher concentrations were conducted with concentrations of 100 mM for the aromatic substrates and 150 mM of N-Boc-Prol (**2**). Subsequently, reactions at lower concentrations were conducted with concentrations of 50 mM for the aromatic substrates and 100 mM of N-Boc-Prol (**2**), in order to consider them as the corresponding reactions at higher concentrations at the time when 50% of the aromatic substrate was consumed.

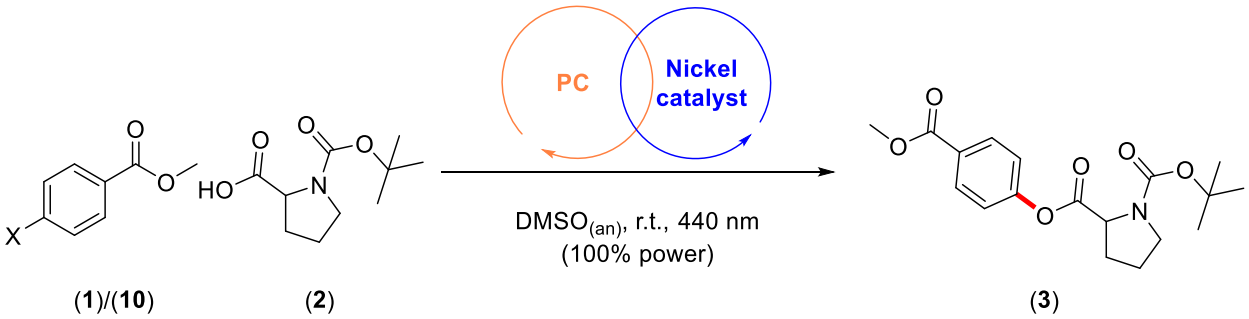

Figure 21: Cross-coupling reaction conducted with the four different catalytic systems

5.1 PRELIMINARY EXPERIMENTS

Before starting the investigation experiments, preliminary reactions were conducted to check whether the photocatalytic systems were able to obtain the product (**3**) from the cross-coupling esterification, without collecting the emission spectra. The test reactions were conducted for each of the four photocatalytic systems, using both aromatic substrates (**1**) and (**10**), maintaining the concentrations that will later be used for the reactions at higher concentrations. An exception was made for single-photocatalytic systems Ni(II)-czbpy (**8**) and poly-Ni(II)-czbpy (**9**); for these procedures, only one test reaction was carried out using only the substrate (**1**) and nucleophile (**2**).

All the results are consistent with those given in literature.[8, 20]

Table 2 Validation experiment scheme for HOMOGENOUS DUAL-PHOTOCATALYTIC SYSTEM Ir(ppy)3 –Ni(II)

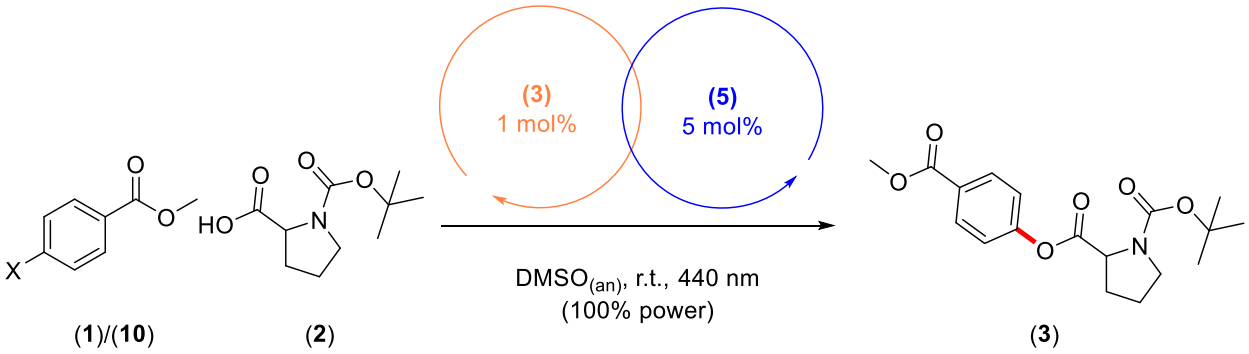

Entry	Substrate	(1)[mM]	(2) [mM]	Conversion (1) [%]	[3] [%]
1	(**1**)	100	150	92%	88%
2	(**10**)	100	150	83%	70%

Reaction conditions: **Entry 1**: 4-methyl-iodobenzoate (300 µmol), *N*-tert-Butoxycarbonyl-L-proline (450 µmol), $Ir(ppy)_3$ (3 µmol), $NiBr_2$diglyme(15 µmol), dtbbpy(15 µmol), $DMSO_{(an)}$ (3 mL), *N*-isopropyl-2-methylpropan-2-amine (900 µmol), 440 nm LED, time 24h. Conversion of 4-methyl-iodobenzoate determined by ^{1}H-NMR using 1,3,5-trimethoxybenzene as internal standard. [c]NMR yields determined by ^{1}H-NMR using 1,3,5-trimethoxybenzene as internal standard. **Entry 2**: 4-methyl-bromobenzoate (300 µmol), *N*-tert-Butoxycarbonyl-L-proline (450 µmol), $Ir(ppy)_3$ (3 µmol), $NiBr_2$diglyme(15 µmol), dtbbpy(15 µmol), $DMSO_{(an)}$ (3 mL), *N*-isopropyl-2-methylpropan-2-amine (900 µmol), 440 nm LED, time 24h. Conversion of 4-methyl-bromobenzoate determined by ^{1}H-NMR using 1,3,5-trimethoxybenzene as internal standard. [c]NMR yields determined by ^{1}H-NMR using 1,3,5-trimethoxybenzene as internal standard.

Table 3 Validation experiment scheme for SEMI-HETEROGENEOUS DUAL-PHOTOCATALYTIC SYSTEM g-CN-OA-m – Nickel(II)

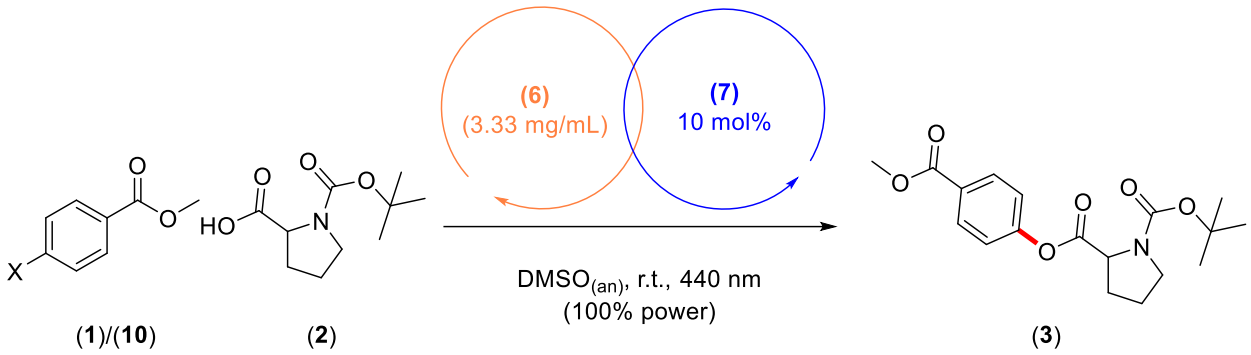

Entry	Substrate	(1)[mM]	(2) [mM]	Conversion (1) [%]	[3] [%]
1	(**1**)	100	150	93%	83%
2	(**10**)	100	150	85%	80%

Reaction conditions: **Entry 1**: 4-methyl-iodobenzoate (300 µmol), *N*-tert-Butoxycarbonyl-L-proline (450 µmol), g-CN-OA-m (10 mg), $NiCl_2$glyme(30 µmol), dtbbpy(30 µmol), $DMSO_{(an)}$ (3 mL), *N*-isopropyl-2-methylpropan-2-amine (900 µmol), 440 nm LED, time 24h. Conversion of 4-methyl-iodobenzoate determined by ^{1}H-NMR using 1,3,5-trimethoxybenzene as internal standard. [c]NMR yields determined by ^{1}H-NMR using 1,3,5-trimethoxybenzene as internal standard. **Entry 2**: 4-methyl-bromobenzoate (300 µmol), *N*-tert-Butoxycarbonyl-L-proline (450 µmol), g-CN-OA-m (10 mg), $NiCl_2$glyme(30 µmol), dtbbpy(30 µmol), $DMSO_{(an)}$ (3 mL), *N*-isopropyl-2-methylpropan-2-amine (900 µmol), 440 nm LED, time 24h. Conversion of 4-methyl-bromobenzoate determined by ^{1}H-NMR using 1,3,5-trimethoxybenzene as internal standard. [c]NMR yields determined by ^{1}H-NMR using 1,3,5-trimethoxybenzene as internal standard.

Table 4 : Validation experiment scheme for HOMOGENOUS SINGLE-PHOTOCATALYTIC SYSTEM Ni(II)-czbpy

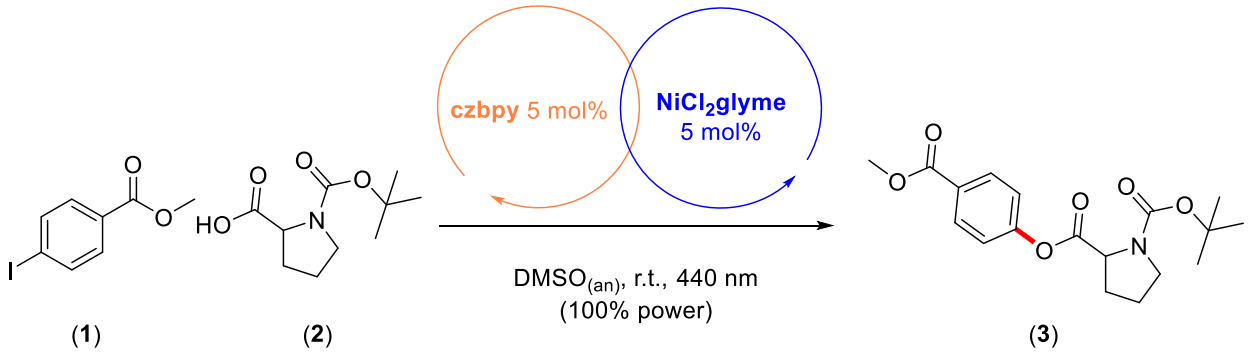

Entry	Substrate	(1)[mM]	(2) [mM]	Conversion (1) [%]	[3] [%]
1	(**1**)	100	150	94%	78%

Reaction conditions: **Entry 1**: 4-methyl-iodobenzoate (300 µmol), *N*-tert-Butoxycarbonyl-L-proline (450 µmol), $NiCl_2$glyme(15 µmol), czbpy(15 µmol), $DMSO_{(an)}$ (3 mL), *N*-isopropyl-2-methylpropan-2-amine (900 µmol), 440 nm LED, time 24h. Conversion of 4-methyl-iodobenzoate determined by ^{1}H-NMR using 1,3,5-trimethoxybenzene as internal standard. [c]NMR yields determined by ^{1}H-NMR using 1,3,5-trimethoxybenzene as internal standard.

Table 5 Validation experiment scheme for HETEROGENEOUS SINGLE-PHOTOCATALYTIC SYSTEM poly-Ni(II)-czbpy

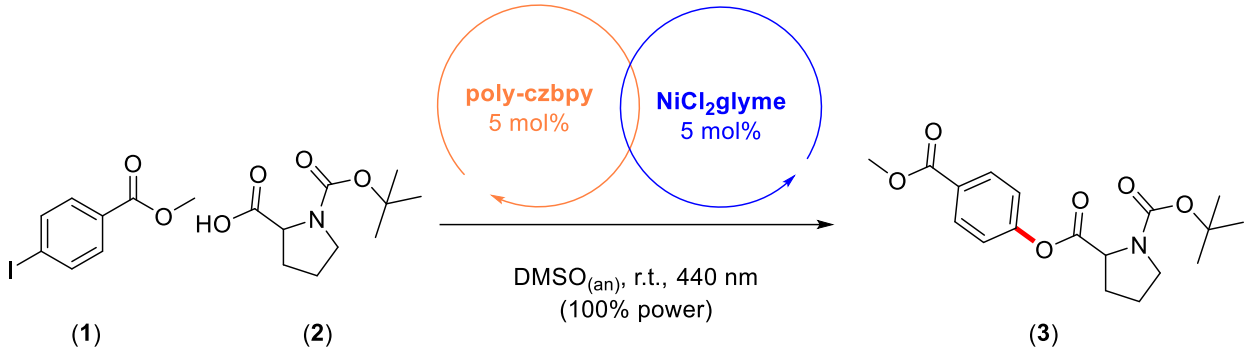

Entry	Substrate	(1)[mM]	(2) [mM]	Conversion (1) [%]	[3] [%]
1	(**1**)	100	150	76%	48%

Reaction conditions: **Entry 1**: 4-methyl-iodobenzoate (300 µmol), *N*-tert-Butoxycarbonyl-L-proline (450 µmol), $NiCl_2$glyme(15 µmol), poly-czbpy(15 µmol), $DMSO_{(an)}$ (3 mL), *N*-isopropyl-2-methylpropan-2-amine (900 µmol), 440 nm LED, time 24h. Conversion of 4-methyl-iodobenzoate/4-methyl-bromobenzoate determined by ^{1}H-NMR using 1,3,5-trimethoxybenzene as internal standard. [c]NMR yields determined by ^{1}H-NMR using 1,3,5-trimethoxybenzene as internal standard.

5.2 REFERENCE PEAKS

For the investigations through the Same Excess Experiments FT-IR emission spectra were continuously collected while a reaction was running. It was possible to observe emission peaks for the aromatic substrates (**1**) and (**10**) and the product (**3**). Since the peculiarity of *in situ* analyses is to collect data continuously, it was possible to derive emission profiles of the compounds involved in the reaction from the systems studied, observing how the substrates were consumed and how the product was generated over time. Two peaks were chosen to follow the variations in time of substrates and product. In order to better identify peaks, the raw spectra were modified, applying differential modifications to the emission data, to enhance their variations over time. The baseline range of reference was chosen to be around 1838 cm^{-1}, by using this wavenumber, no sensible differences in emission spectra are observed over the time studied (Table 6).

For the emission peaks identified, it was possible to monitor their progression over time.

At the end of each reaction, NMR analysis was performed to quantify the amount of compounds in solution using an internal standard (1,3,5-trimethoxybenzene). Emission profiles were converted to concentration profiles, so that the amount of compounds could be quantified and Same Excess experiments could be completed by overlaying the substrate consumption graphs (Figure 22).

Table 6: Identification on the derivative spectra of the reference peak for the substrate (**1**) and (**10**) and of product (**3**)

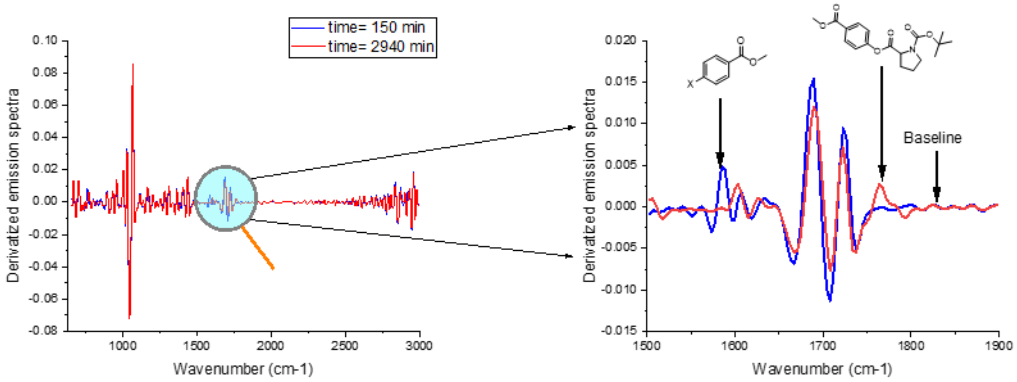

Compound	Absorption range [cm^{-1}]	Lit. Absorption [cm^{-1}]
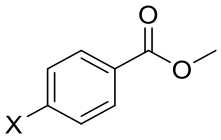	1579-1589	1580 (aromatic stretching transition v_{CC}, weak)[41]
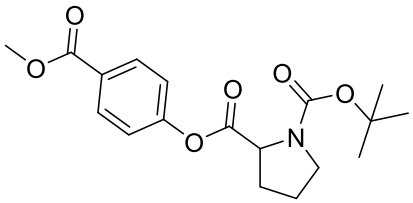	1761-1771	1765 (carbon-oxygen stretching v_{co}, weak)[42]

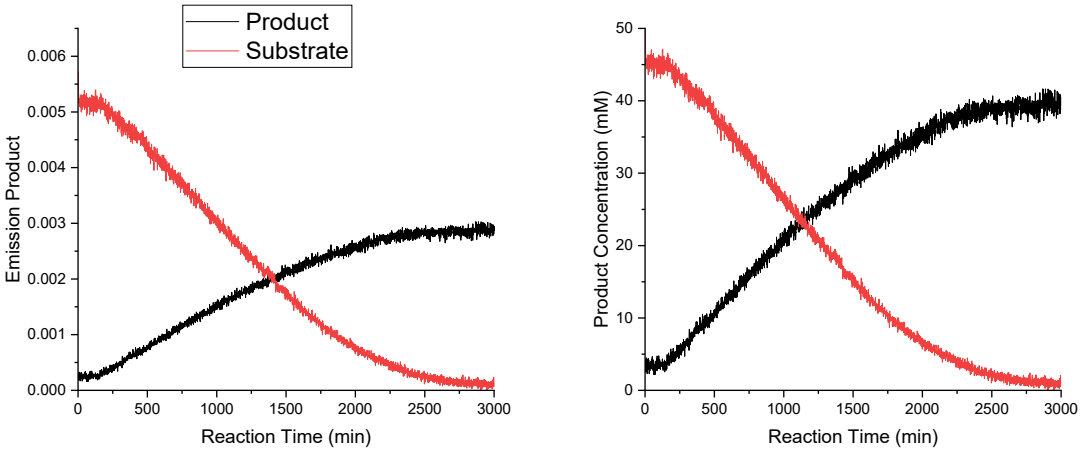

Figure 22: Reported the graphs of the emission (left) and the elaborated showing the concentration (right)

5.3 TECHNIQUE VALIDATION

In order to use the FT-IR technique as an *in situ* analysis to visualize the progress of the reaction, it was necessary to validate that the technique provides accurate data on the concentrations of reagents and products. This experiment is fundamental to verify if the conversion from the emission data to the concentration data maintains the linear proportionality in the whole concentration range where the compounds are analyzed. Therefore, an *ex situ* analysis of a reaction, monitored *in situ* with the FTIR technique, was carried out. In this test reaction, the photocatalytic homogeneous system Ir(ppy)3 -Ni(II) was included with the substrate (**1**), together with an equal molar amount of 1,3,5-trimethoxybenzene. This photocatalytic system was chosen because it enables the substrate to be converted in a short time. During the reaction period, every 15 minutes an aliquot was withdrawn and submitted to 1H-NMR analysis. The calculated IR yields were found to be consistent with the determined 1H-NMR yields with minor deviations, visualized as an overlay. The consistency in data of the two independent methods indicates that ReactIR collected data are valid and reproducible, both for the substrates and product signals (Table 7).

Table 7: Technique validation experiment scheme

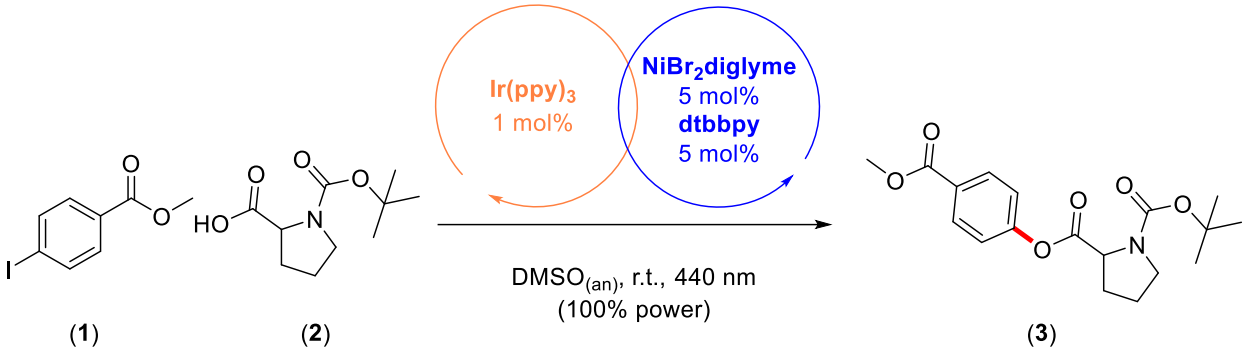

Entry	Substrate	(1)[mM]	(2) [mM]	Conversion (1) [%]	[3] [%]
1	(**1**)	50	100	92%	88%

Reaction conditions: **Entry 1**: 4-methyl-iodobenzoate (150 µmol), *N*-tert-Butoxycarbonyl-L-proline (300 µmol), $Ir(ppy)_3$ (3 µmol), $NiBr_2$diglyme(15 µmol), dtbbpy(15 µmol), $DMSO_{(an)}$ (3 mL), *N*-isopropyl-2-methylpropan-2-amine (900 µmol), 440 nm LED, time 90 min. Conversion of 4-methyl-iodobenzoate determined by ^{1}H-NMR using 1,3,5-trimethoxybenzene as internal standard. [c]NMR yields determined by ^{1}H-NMR using 1,3,5-trimethoxybenzene as internal standard.

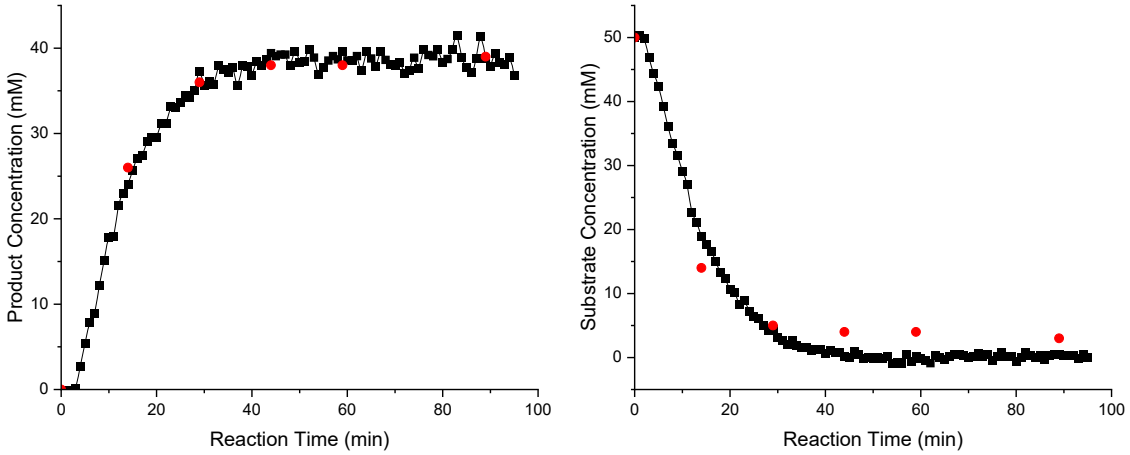

Time [min]	(3) IR [mM]	(3) NMR [mM]	Deviation (%)	(1) IR [mM]	(1) NMR [mM]	Deviation (%)
0	0	0	0	50	50	0
15	24	26	8	19	14	26
30	37	36	3	4	9	44
45	39	38	3	4	5	20
60	40	38	5	0	4	-
90	39	39	0	0	3	-

5.4 INVESTIGATIONS

5.4.1 INVESTIGATION OF THE SYSTEM $Ir(ppy)_3$ –Nickel(II)

The use of the photocatalyst $Ir(ppy)_3$ (**3**) in combination with the Nickel complex (**5**) results in high product yields. This procedure can be applied for both the aromatic substrates Ar-I (**1**)[34] and Ar-Br (**10**)[8]. This investigation is essential to corroborate or disprove the procedure, since as demonstrated by Pieber and coworkers, the corresponding cross-coupling amination reaction, with an electron-poor aromatic substrate requiring an iridium complex as homogeneous photocatalyst, causes catalyst degradation with nickel-black formation. This problem has been circumvented by decreasing the photocatalyst/nickel catalyst ratio; in this new condition, no nickel black is formed, since the rate of additive oxidation is greater than or equal to that of reductive elimination, preventing the nickel(0) metal from agglomerating.[8, 26]

From the two graphs of the Same-Excess experiments it can be seen that for both substrates (**1**) (Table 9) and (**10**) (Table 10) there is neither product deactivation nor catalyst degradation, as in both cases there is an overlap between the two graphs. These results suggest that there is no large difference between the reaction rates of reductive elimination and oxidative addition, independently by the used substrate.

Table 8

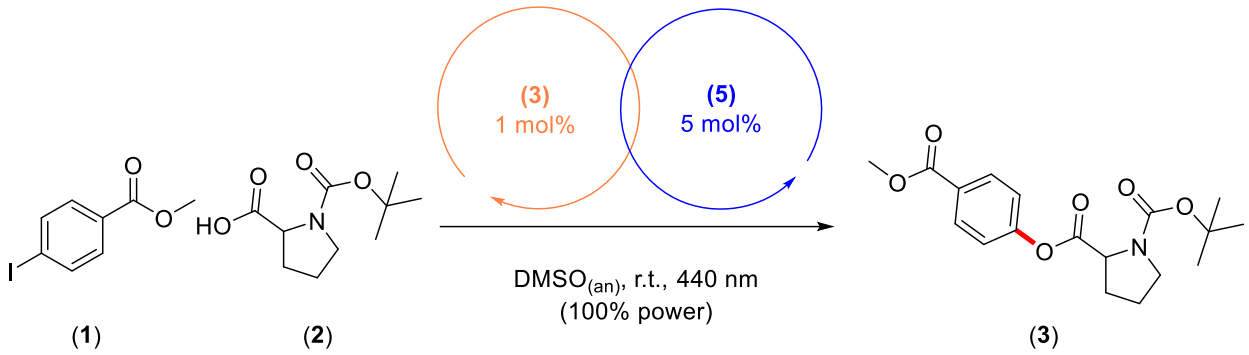

Entry	(1) [mM]	(2) [mM]	(2)-(1) [mM]	Conversion (1) [%]	[3] [%]
1	100	150	50	96	89
2	50	100	50	97	84

Reaction conditions: **Entry 1**: 4-methyl-iodobenzoate (300 µmol), *N*-tert-Butoxycarbonyl-L-proline (450 µmol), $Ir(ppy)_3$ (3 µmol), $NiBr_2$diglyme(15 µmol), dtbbpy(15 µmol), $DMSO_{(an)}$ (3 mL), *N*-isopropyl-2-methylpropan-2-amine (900 µmol), 440 nm LED, time 19h. Conversion of 4-methyl-iodobenzoate/4-methyl-bromobenzoate determined by ^{1}H-NMR using 1,3,5-trimethoxybenzene as internal standard. [c]NMR yields determined by ^{1}H-NMR using 1,3,5-trimethoxybenzene as internal standard. **Entry 2**: 4-methyl-iodobenzoate (150 µmol), *N*-tert-Butoxycarbonyl-L-proline (300 µmol), $Ir(ppy)_3$ (3 µmol), $NiBr_2$diglyme(15 µmol), dtbbpy(15 µmol), $DMSO_{(an)}$ (3 mL), *N*-isopropyl-2-methylpropan-2-amine (900 µmol), 440 nm LED, time 16h. Conversion of 4-methyl-iodobenzoate determined by ^{1}H-NMR using 1,3,5-trimethoxybenzene as internal standard. [c]NMR yields determined by ^{1}H-NMR using 1,3,5-trimethoxybenzene as internal standard.

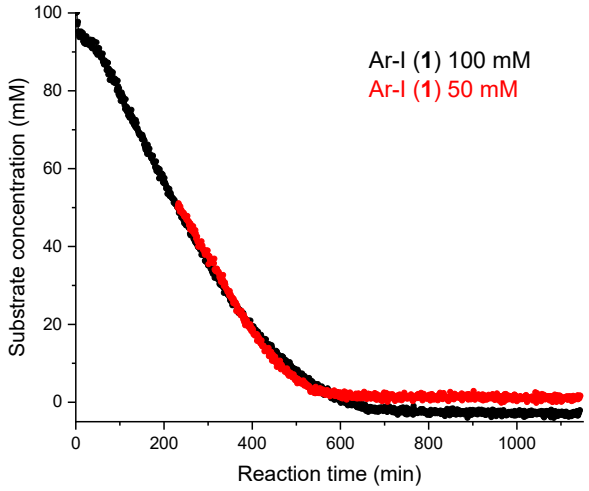

Table 9

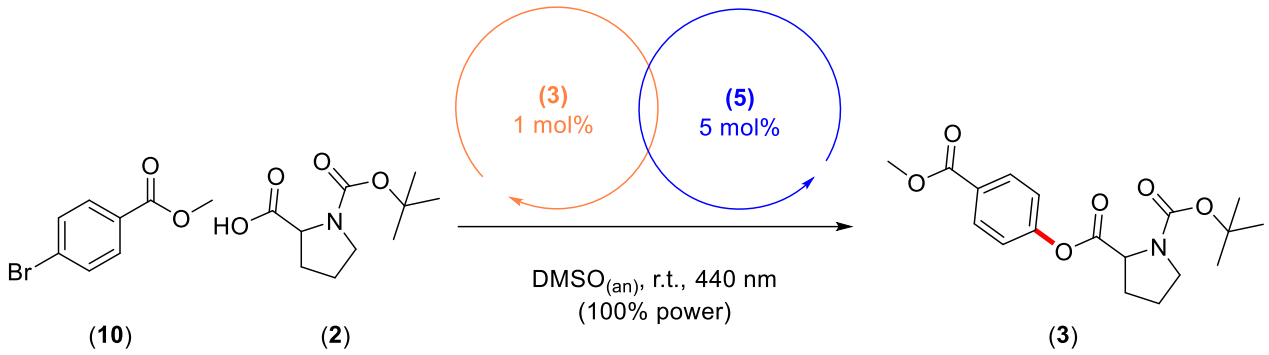

Entry	(10) [mM]	(2) [mM]	(2)-(10) [mM]	Conversion (1) [%]	[3] [%]
1	100	150	50	86	79
2	50	100	50	84	74

Reaction conditions: **Entry 1**: 4-methyl-bromobenzoate (300 µmol), *N*-tert-Butoxycarbonyl-L-proline (450 µmol), $Ir(ppy)_3$ (3 µmol), $NiBr_2$diglyme(15 µmol), dtbbpy(15 µmol), $DMSO_{(an)}$ (3 mL), *N*-isopropyl-2-methylpropan-2-amine (900 µmol), 440 nm LED, time 75h. Conversion of 4-methyl-iodobenzoate/4-methyl-bromobenzoate determined by ^{1}H-NMR using 1,3,5-trimethoxybenzene as internal standard. [c]NMR yields determined by ^{1}H-NMR using 1,3,5-trimethoxybenzene as internal standard. **Entry 2**: 4-methyl-bromobenzoate (150 µmol), *N*-tert-Butoxycarbonyl-L-proline (300 µmol), $Ir(ppy)_3$ (3 µmol), $NiBr_2$diglyme(15 µmol), dtbbpy(15 µmol), $DMSO_{(an)}$ (3 mL), *N*-isopropyl-2-methylpropan-2-amine (900 µmol), 440 nm LED, time 67h. Conversion of 4-methyl-bromobenzoate determined by ^{1}H-NMR using 1,3,5-trimethoxybenzene as internal standard. [c]NMR yields determined by ^{1}H-NMR using 1,3,5-trimethoxybenzene as internal standard.

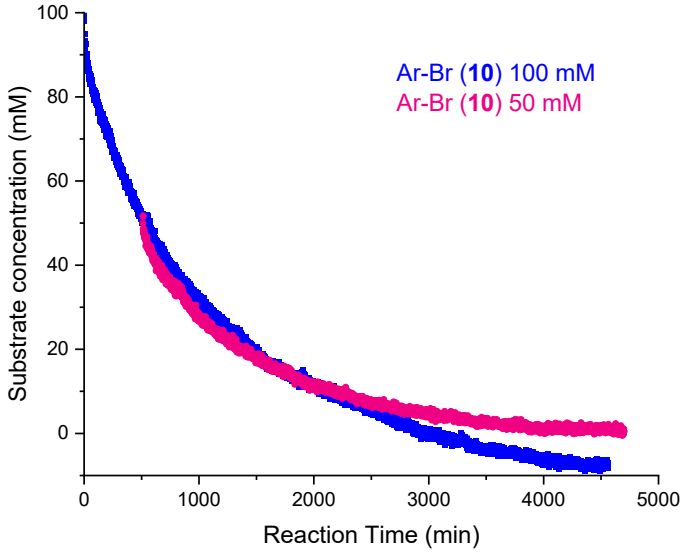

5.4.2 INVESTIGATION OF THE SYSTEM g-CN-OA-m–Nickel(II)

In the analysis carried out for the semi-heterogeneous catalytic system g-CN-OA-m-Nickel(II) neither product deactivation nor catalyst degradation were detected. This is reported for both types of aromatic substrate (**1**) (Table 10) and (**10**) (Table 11). This confirms that the procedures are suitable for application in cycles, in which the heterogeneous photocatalyst (**6**) does not undergo a catalyst degradation phenomenon. The experimental data suggest that, despite the fact that compound (**6**) is a worse reductant than (**4**) (E=-1.73 V for (**4**) and E=-1.65 V for (**6**))[34], the oxidative addition of a possible aromatic radical anion can still take place at comparable kinetics to the reductive elimination.[34]

Table 10

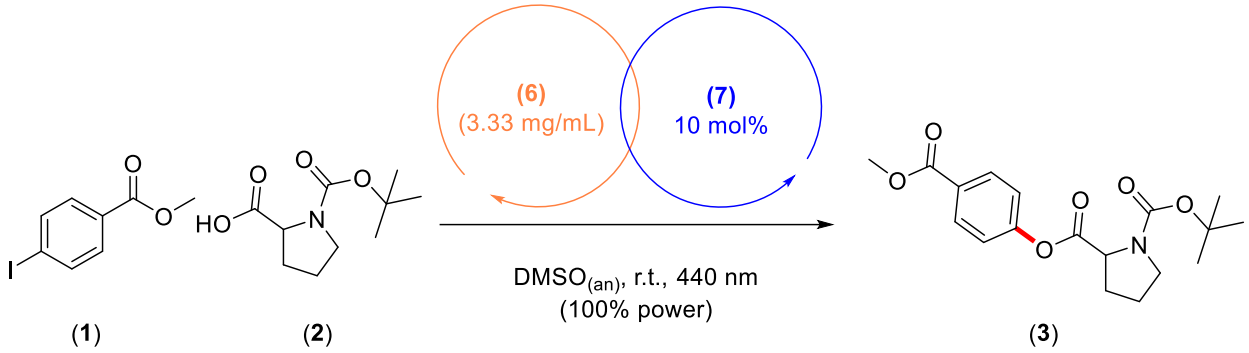

Entry	(1) [mM]	(2) [mM]	(2)-(1) [mM]	Conversion (1) [%]	[3] [%]
1	100	150	50	86	78
2	50	100	50	84	74

Reaction conditions: **Entry 1**: 4-methyl-iodobenzoate (300 µmol), *N*-tert-Butoxycarbonyl-L-proline (450 µmol), g-CN-OA-m (10 mg), $NiCl_2$glyme(30 µmol), dtbbpy(30 µmol), $DMSO_{(an)}$ (3 mL), *N*-isopropyl-2-methylpropan-2-amine (900 µmol), 440 nm LED, time 20h. Conversion of 4-methyl-iodobenzoate determined by ^{1}H-NMR using 1,3,5-trimethoxybenzene as internal standard. [c]NMR yields determined by ^{1}H-NMR using 1,3,5-trimethoxybenzene as internal standard. **Entry 2**: 4-methyl-iodobenzoate (150 µmol), *N*-tert-Butoxycarbonyl-L-proline (300 µmol), g-CN-OA-m (10 mg), $NiCl_2$glyme(30 µmol), dtbbpy(30 µmol), $DMSO_{(an)}$ (3 mL), *N*-isopropyl-2-methylpropan-2-amine (900 µmol), 440 nm LED, time 15h. Conversion of 4-methyl-iodobenzoate determined by ^{1}H-NMR using 1,3,5-trimethoxybenzene as internal standard. [c]NMR yields determined by ^{1}H-NMR using 1,3,5-trimethoxybenzene as internal standard.

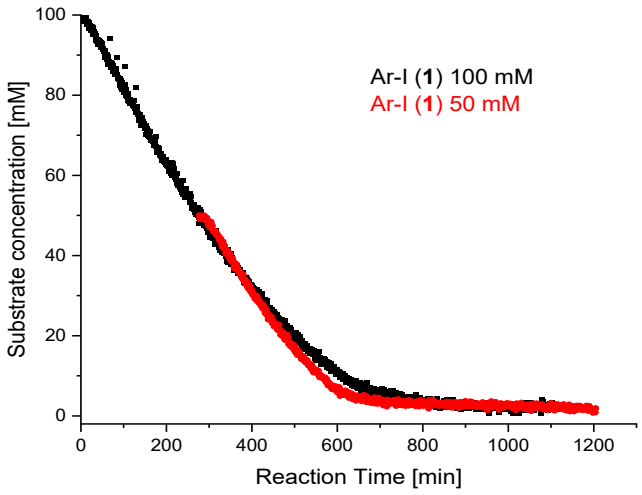

Table 11

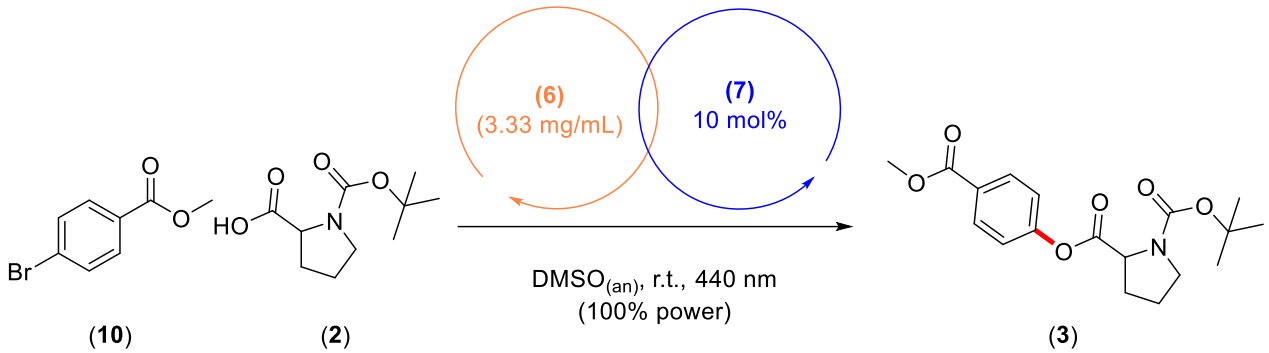

(**10**) (**2**) (**3**)

Entry	(10) [mM]	(2) [mM]	(2)-(10) [mM]	Conversion (1) [%]	[3] [%]
1	100	150	50	96	89
2	50	100	50	94	84

Reaction conditions: **Entry 1**: 4-methyl-bromobenzoate (300 µmol), *N*-tert-Butoxycarbonyl-L-proline (450 µmol), g-CN-OA-m (10 mg), $NiCl_2$glyme(30 µmol), dtbbpy(30 µmol), $DMSO_{(an)}$ (3 mL), *N*-isopropyl-2-methylpropan-2-amine (900 µmol), 440 nm LED, time 71h. Conversion of 4-methyl-bromobenzoate determined by ^{1}H-NMR using 1,3,5-trimethoxybenzene as internal standard. [c]NMR yields determined by ^{1}H-NMR using 1,3,5-trimethoxybenzene as internal standard. **Entry 2**: 4-methyl-bromobenzoate (150 µmol), *N*-tert-Butoxycarbonyl-L-proline (300 µmol), g-CN-OA-m (10 mg), $NiCl_2$glyme(30 µmol), dtbbpy(30 µmol), $DMSO_{(an)}$ (3 mL), *N*-isopropyl-2-methylpropan-2-amine (900 µmol), 440 nm LED, time 46h. Conversion of 4-methyl-bromobenzoate determined by ^{1}H-NMR using 1,3,5-trimethoxybenzene as internal standard. [c]NMR yields determined by ^{1}H-NMR using 1,3,5-trimethoxybenzene as internal standard.

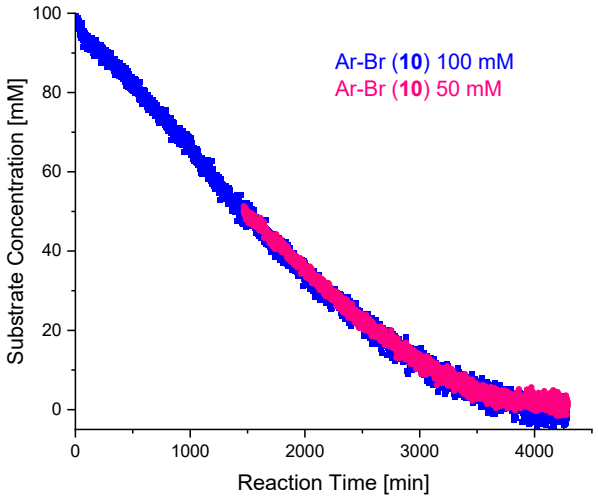

5.4.3 INVESTIGATION OF THE SYSTEM Ni(II)-czbpy

The graphs of the experiments for the catalyst (**8**) showed no kinetic drop (Table 12). This is a good result, as it implies that the newly developed catalyst has uniform kinetics in the mechanisms of its cycle.

Table 12

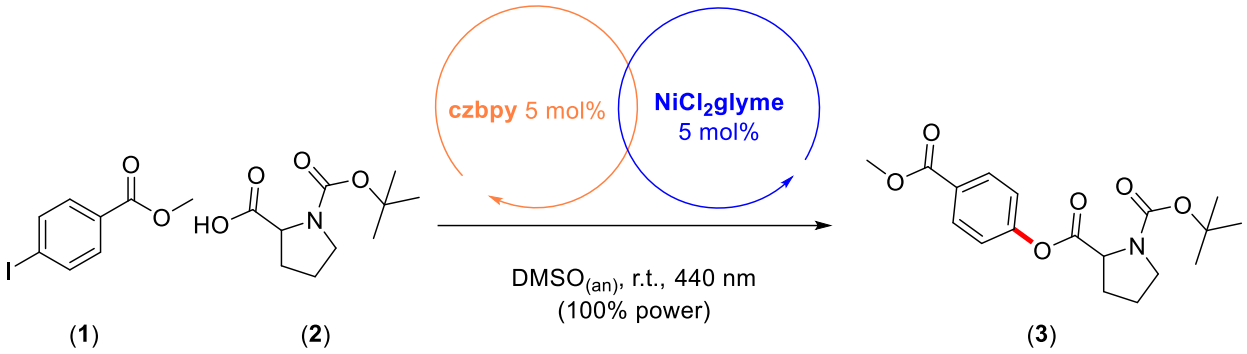

Entry	(1) [mM]	(2) [mM]	(2)-(1) [mM]	Conversion (1) [%]	[3] [%]
1	100	150	50	86	78
2	50	100	50	84	74

Reaction conditions: **Entry 1**: 4-methyl-iodobenzoate (300 µmol), *N*-tert-Butoxycarbonyl-L-proline (450 µmol), $NiCl_2$glyme(15 µmol), czbpy (15 µmol),, $DMSO_{(an)}$ (3 mL), *N*-isopropyl-2-methylpropan-2-amine (900 µmol), 440 nm LED, time 24h. Conversion of 4-methyl-iodobenzoate/4-methyl-bromobenzoate determined by ^{1}H-NMR using 1,3,5-trimethoxybenzene as internal standard. [c]NMR yields determined by ^{1}H-NMR using 1,3,5-trimethoxybenzene as internal standard. **Entry 2**: 4-methyl-iodobenzoate (150 µmol), *N*-tert-Butoxycarbonyl-L-proline (300 µmol), $NiCl_2$glyme(15 µmol), czbpy(15 µmol),, $DMSO_{(an)}$ (3 mL), *N*-isopropyl-2-methylpropan-2-amine (900 µmol), 440 nm LED, time 24h. Conversion of 4-methyl-iodobenzoate/4-methyl-bromobenzoate determined by ^{1}H-NMR using 1,3,5-trimethoxybenzene as internal standard. [c]NMR yields determined by ^{1}H-NMR using 1,3,5-trimethoxybenzene as internal standard.

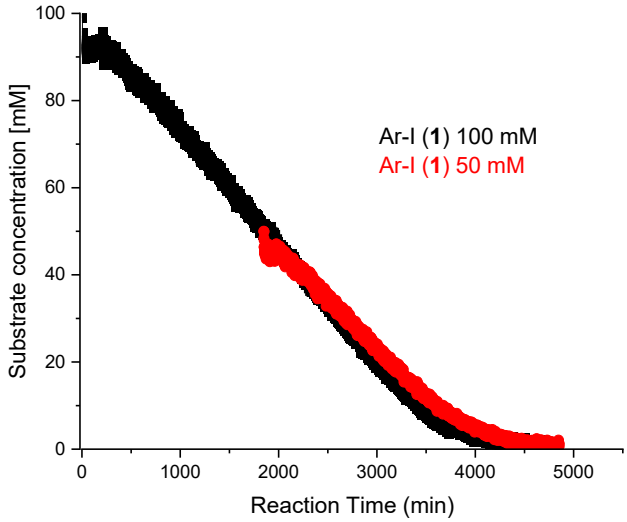

5.4.4 INVESTIGATION OF THE SYSTEM poly-Ni(II)-czbpy

When using the binder polymer (**9**) as a photocatalyst, it was observed that the two reaction progress profiles did not overlap (Table 13). This led to a third experiment, which was reproduced with the same amount of reagents and product as the second experiment (Table 14). From the third experiment, it was observed that there was no coincidence between the concentration values of the products during the reaction time, indicating that the catalyst was deactivated during the process. Possible explanations are reported in the next sections.

Table 13

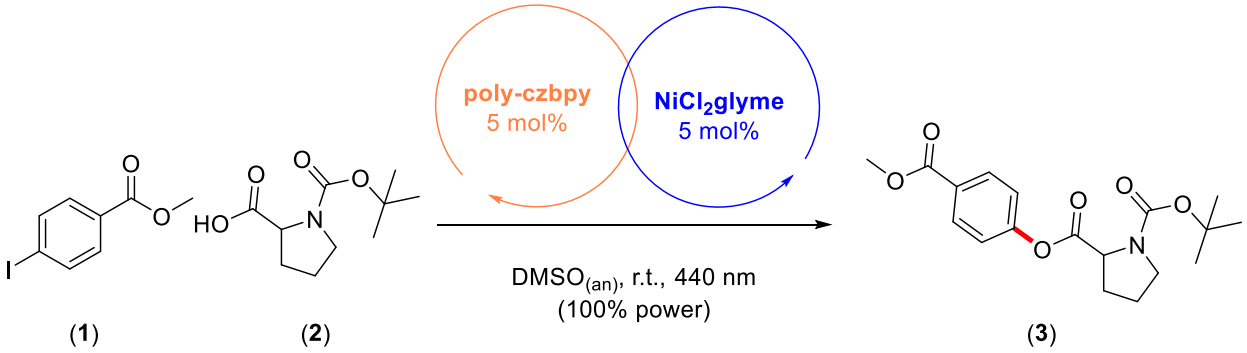

Entry	(1) [mM]	(2) [mM]	(2)-(1) [mM]	Conversion (1) [%]	[3] [%]
1	100	150	50	72	51
2	50	100	50	74	49

Reaction conditions: **Entry 1**: 4-methyl-iodobenzoate (300 µmol), *N*-tert-Butoxycarbonyl-L-proline (450 µmol), $NiCl_2$glyme(15 µmol), poly-czbpy(15 µmol), $DMSO_{(an)}$ (3 mL), *N*-isopropyl-2-methylpropan-2-amine (900 µmol), 440 nm LED, time 24h. Conversion of 4-methyl-iodobenzoate/4-methyl-bromobenzoate determined by ^{1}H-NMR using 1,3,5-trimethoxybenzene as internal standard. [c]NMR yields determined by ^{1}H-NMR using 1,3,5-trimethoxybenzene as internal standard. **Entry 2**: 4-methyl-iodobenzoate (150 µmol), *N*-tert-Butoxycarbonyl-L-proline (300 µmol), $NiCl_2$glyme(15 µmol), poly-czbpy(15 µmol),, $DMSO_{(an)}$ (3 mL), *N*-isopropyl-2-methylpropan-2-amine (900 µmol), 440 nm LED, time 24h. Conversion of 4-methyl-iodobenzoate/4-methyl-bromobenzoate determined by ^{1}H-NMR using 1,3,5-trimethoxybenzene as internal standard. [c]NMR yields determined by ^{1}H-NMR using 1,3,5-trimethoxybenzene as internal standard.

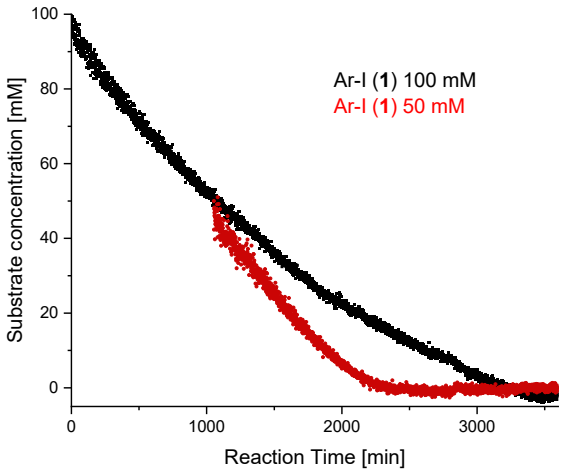

Table 14

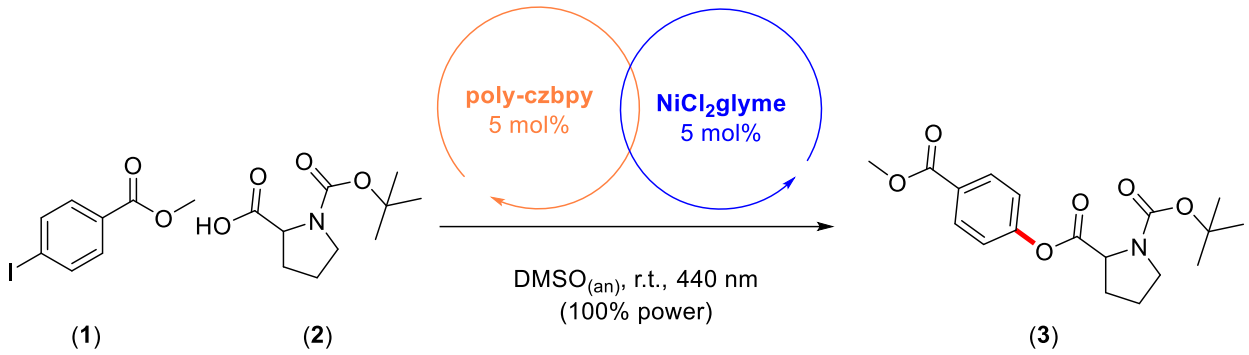

Entry	(1) [mM]	(2) [mM]	(3) [mM]	(2)-(1) [mM]	Conversion (1) [%]
3	50	100	0	50	65
4	50	100	50	50	30

Reaction conditions: **Entry 3**: 4-methyl-iodobenzoate (41.10 µmol), *N*-tert-Butoxycarbonyl-L-proline (82.21 µmol), $NiCl_2$glyme(0.53 µmol), poly-czbpy(0.53 µmol), $DMSO_{(an)}$ (0.82 mL), *N*-isopropyl-2-methylpropan-2-amine (39.1 µmol), 440 nm LED, time 90 min. Conversion of 4-methyl-iodobenzoate determined by ^{1}H-NMR using 1,3,5-trimethoxybenzene as internal standard. [c]NMR yields determined by ^{1}H-NMR using 1,3,5-trimethoxybenzene as internal standard. **Entry 4**: 4-methyl-iodobenzoate (10.77 µmol), *N*-tert-Butoxycarbonyl-L-proline (82.21 µmol), $NiCl_2$glyme(0.53 µmol), poly-czbpy(0.53 µmol),, $DMSO_{(an)}$ (0.82 mL), *N*-isopropyl-2-methylpropan-2-amine (39.1 µmol), 1-(tert-butyl) 2-(4-methoxycarbonyl)phenyl)pyrrolidine-1,2-dicarboxylate (41.10 µmol), 440 nm LED, time 90 min. Conversion of 4-methyl-iodobenzoate determined by ^{1}H-NMR using 1,3,5-trimethoxybenzene as internal standard. [c]NMR yields determined by ^{1}H-NMR using 1,3,5-trimethoxybenzene as internal standard.

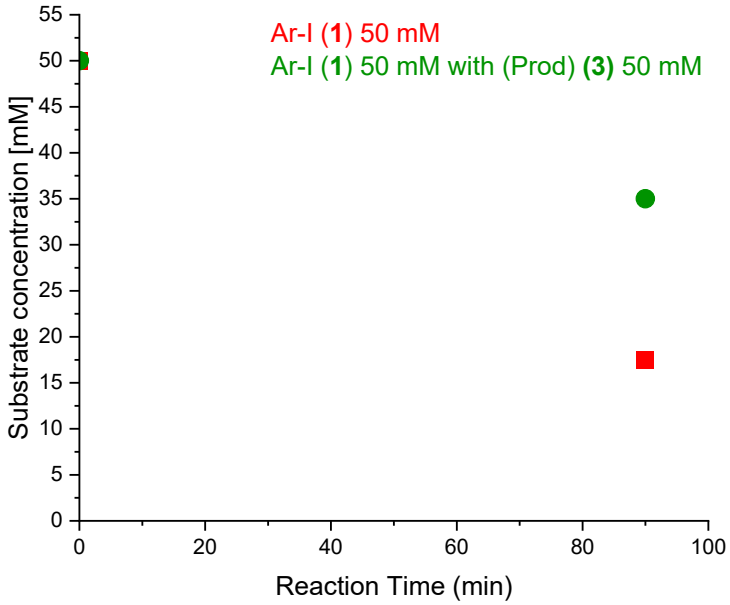

5.4.4.1 DIFFERENCES IN REACTION RATES BETWEEN OXIDATIVE ADDITION AND REDUCTIVE ELIMINATION

The first hypothesis is that the reductive elimination process is faster than the oxidative addition, as the former is photocatalyzed. This hypothesis should be verified if in the catalytic cycle, between the oxidative addition and reductive elimination processes, there are additional excitation phenomena by the ligands.[26]

5.4.4.2 DIFFERENCES IN REACTION RATES BETWEEN INTERMOLECULAR AND INTRAMOLECULAR REACTIONS

The second hypothesis is that the kinetics of intramolecular and intermolecular processes are different; the latter is particularly slower because it requires a bimolecular collision phenomenon. In the particular case of this cross-coupling reaction, this is statistically less favorable, since the catalytic site is immobilized on the polymeric support, reducing the catalyst freedom degree and thus lowering the probability of a favorable collision between the nickel core and the aromatic substrate.[26] Because of this, the number of oxidative additions is lower than the number of reductive eliminations, leading to an accumulation of nickel species with low oxidation numbers such as Ni(I) and Ni(0).

5.4.4.3 SUPPORT AMINE ACTIVITY

The third hypothesis relies on the presence of a large stoichiometric amount of base. The amine is needed to coordinate the nickel complexes and promote catalytic action, but it also has reductive capabilities, so it may keep the oxidation status of the nickel sites low. The base could act as a reductant in catalytic cycle processes with photoredox mechanism, reducing the high valence Nickel species to low valence Nickel species and enhancing the rate of reductive elimination. Furthermore the nucleophile amine can bind the low valence sites, having an opposite effect, stabilizing the Nickel species which cannot degrade to Nickel black.[34]

5.4.4.4 LOWER REDUCTION POTENTIAL OF PHOTOEXCITED poly-Ni(II)-czbpy SYSTEM

The fourth speculation is that the solid photocatalyst, in which the Nickel sites are anchored, may have a lower reduction potential than its monomeric Ni(II)-czbpy counterpart, increasing the accumulation of low-oxidation-state nickel in the system by giving electrons to the Ni(II) pre-catalytic species. If the photoexcitation of the ligand reduces the nickel core by an electron transfer process, it can be assumed that this mechanism may be more favored, since as the extent of the conjugated system increases also the energy of the HOMO increases, thus making it easier to form an electronic vacancy in the polymer structure.

Also in the polymeric conjugated structure of the photocatalyst the charge can move very easily. [43-44] A circumstantial evidence for this hypothesis can be found by comparing the kinetic curve of the Same-Excess experiments in the case of Ni(II)-czbpy and poly-Ni(II)-czbpy. In the case of Ni(II)-czbpy it can be observed that an induction time is present, which can be attributed to the time required for the catalyst to be activated (Figure 23). Since this is not observed in the graphs of poly-Ni(II)-czbpy, it can be assumed that this delay is not due to the oxidative addition between the nickel and the aromatic substrate (as stated above), but to the formation of enough active catalyst by photoexcitation.

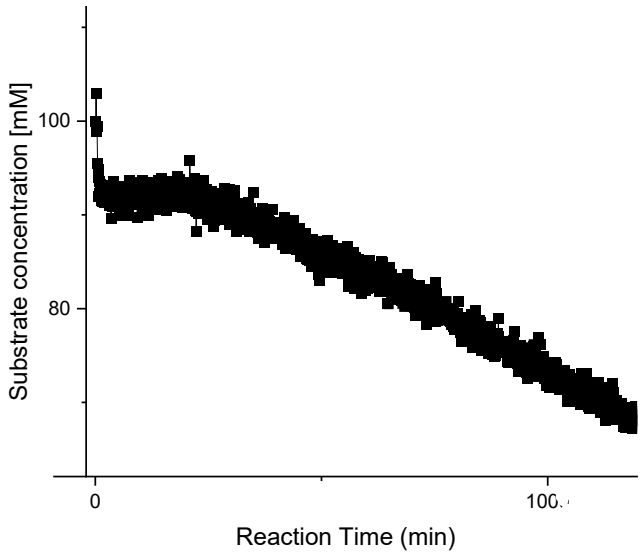

Figure 23 Presence of induction time in the Ni(II)-czbpy kinetic curve

6. CONCLUSIONS

During this project, the Same Excess Experiment technique was used to check the robustness of photocatalytic systems. The Same Excess Experiments provided easily interpretable information on the catalytic systems investigated. This makes this technique particularly advantageous, as it can be used as a screening analysis to determine whether catalytic systems are susceptible to influence from factors that may reduce their efficiency. The project was started with a series of experiments to check whether the procedures reported in the reference literature were reliable. Subsequently, it was evaluated whether the Same Excess Experiment technique coupled with *in situ* analysis using FT-IR spectroscopy was able to reveal the presence of catalyst degradation or product inhibition.

These tests showed that the technique was not only suitable for these purposes but that the data provided was also accurate and consistent.

In the case of the $Ir(ppy)_3$ –Nickel(II), g-CN-OA-m – Nickel(II) and Ni(II)-czbpy systems, it was observed that there is neither catalytic deactivation nor product inhibition. These results are in line with the theory that precipitation of nickel metal by the catalyst occurs when the substrate is not sufficiently electropositive, making oxidative addition slow. The presence of electron-withdrawing groups on the aromatic substrate favors oxidative addition, making it not kinetically disadvantaged, compared to reductive elimination of the nickel complex.[26]

In the case of the system poly-Ni(II)-czbpy, however, catalytic degradation was observed, which can be traced back to a possible precipitation of nickel metal.[26] As the mechanism is unclear, it is difficult to determine the real cause of this deactivation, requiring further mechanistic investigations.

7. OUTLOOK

Future *in situ* monitoring analyses should verify whether there is catalytic degradation in the $Ir(ppy)_3$ – Nickel(II), g-CN-OA-m – Nickel(II) and Ni(II)-czbpy systems, using electron-poor aromatic substrates. If the catalytic degradation is worse in these cases than those measured in this thesis, it would mean that there is low oxidative addition in the mechanism of cross-coupling esterification. Furthermore, other studies should be done to understand if there is catalytic degradation in amination cross-coupling reactions with different photocatalysts.

It is necessary to identify the mechanism beyond the catalyst degradation, to develop strategies to reduce this phenomena in the photocatalytic system poly-Ni(II)-czbpy. This heterogeneous photocatalyst belongs to a new generation of heterogeneous photocatalysts with the promising potential of not requiring second compounds to act as photocatalyst. Future *In situ* analyses should study if there is catalytic deactivation using irradiation with light at longer wavelengths. Previous studies have reported that the formation of Nickel black was decreased using longer wavelengths for the C-N cross-coupling with electron-poor substrates.[26] This experiment aims to understand if the reductive elimination is slowed down, minimizing the accumulation of low valence Nickel species.

Another possible extension of this thesis could be the study of the effects of increasing the concentration of the aromatic substrate in the reaction mixture, to observe if there is a variation in the catalytic degradation phenomenon. A major amount of substrate molecules should also increase the quantity of oxidative addition phenomena between them and the polymer-bounded Nickel sites. It should be studied, if the same principle applies, when using heterogeneous photocatalyst with a larger surface area and, if that leads to a minor catalytic degradation phenomenon.

It would be also interesting to verify if the catalytic degradation persists when using a secondary amine as base, with different reduction potential and nucleophilicity. These analyses could figure out if the base can act as a nucleophile to stabilize the low nickel species, preventing them from merging into Nickel black or, on the contrary, the base can act as reductant agent to reduce the nickel species to nickel black.

Finally, it should be verified if by changing the structure of the polymeric ligand and increasing its reduction potential the catalytic degradation decreases, which in turn should cause a decrease in the formation of low nickel species. A possible modification could be the addition of electron-withdrawing groups to the aromatic moieties of the polymer.

8. EXPERIMENTAL PART

8.1 GENERAL REMARKS

Substrates, reagents and solvent were purchased from commercial suppliers and used, if not otherwise noted, without further purification. N-Boc proline was lyophilized and stored under nitrogen atmosphere. N-tert-butylisopropylamine (BIPA) was synthesized according to literature procedure. 1H-NMR spectra were obtained using a Varian 400 spectrometer (400 MHz, Agilent) and an Ascend 400 spectrometer (400 MHz, Bruker) and are reported in ppm relative to the residual solvent peaks. NMR analysis was used for quantification through Varian 400 MHz spectrometer and a Varian 600 MHz spectrometer with the following settings: acquisition points (complex points) 16384, Acquisition time 2.556 s, relaxation delay 1.00 s, receiver gain as autogain (default 30), spectral width 15 ppm, 64 scans. Peaks are reported as: s = singlet, d = doublet, t = triplet, m = multiplet or unresolved. Coupling constants are reported in Hz. Lamps (A160, 40 W maximum) were purchased from Kessil. In situ FTIR analysis was performed with a ReactIRTM 15 (Mettler-Toledo) console with a DST 9.5 mm SiComp probe attached. Data obtained from the iCiR were processed in Microsoft Excel and presented in Origin (OriginPro 2021). The UV-Vis spectra of g-CN-OA-m was recorded using a UV-2600 spectrometer "Shimadzu" equipped with an integrating sphere.

8.2 GENERAL PROCEDURES AND ANALYSES FOR *in situ* FTIR EXPERIMENTS

8.2.1 CONSIDERATION BEFORE EXPERIMENTS

Before each experiment, the ReactIR console was filled with liquid nitrogen and refilled twice a day to ensure its temperature was constant. When the reaction mixture was ready, the vessel was attached to the probe, then the background spectrum was recorded. To exclude any errors deriving from inconsistent lamp distance and orientation, the Kessil lamp (400 nm) was permanently affixed to a metal rod, maintaining a distance between the light source and the middle of the diameter of the ReactIR probe of 3.5 cm. All reactions were carried out at maximum stirring speed.

8.2.2 GENERAL EXPERIMENTAL PROCEDURE

For each experiment a dried-oven-custom-made vial with an attached sidearm (19 x 100 mm) was loaded with a magnetic stir bar, N-Boc proline (**2**), the respective aryl halides 4-methyl-iodobenzoate (**1**) or 4-methyl-bromobenzoate (**10**), the photocatalyst, the nickel catalysts (**5**) and (**7**) and from a stock solution for the experiments with the combination of $Ir(ppy)_3$ (**4**) and g-CN-OA-m (**6**). For the reactions with czbpy (**8**) and poly-czbpy (**9**), 3 mL of anhydrous DMSO and BIPA were added together with the Nickel(II) chloride

ethylene glycol dimethyl ether complex directly into the vessels. Both necks of the vial were sealed with septa and Parafilm. To ensure fine dispersion of the reaction mixture was sonicated for 5 min and following this was stirred for 5-10 minutes.

The vial was then connected to the ReactIR probe and degassed with nitrogen for 10 min through a needle inserted through the side neck. After 2 min of shaking, to re-assure mixing, while collecting data, the iCiR software was started and the lamp was switched on at 100% power.

The reactions were considered over when both the reaction profiles acquired of product and substrate arrived at a plateau situation. After that, an equal molar amount of 1,3,5-trimethoxibenzene was added to the reaction mixture and sonicated for 2 minutes. After the sonication, a small aliquot of reaction (~10 µL) was extracted and added in a NMR tube with 50 µL deuterated dimethyl sulfoxide.

8.2.3 CONSIDERATIONS AFTER EXPERIMENTS

For each experiment, a single-point baseline of 1838 cm^{-1} was set in the iCIR software to measure the substrate (**1**) and (**10**) consumption, and at 1765 cm^{-1} to measure product generation. Raw data collected by iCiR were exported and processed using Origin.

8.2.4 CONSIDERATIONS ABOUT THE LAMP

Batch experiments with blue light were performed using the same lamp, model Kessil PR160L-440 LED. The reaction vessels were placed on a stirring plate 4.5 cm away from a single lamp. To avoid heating the reaction mixture, a cooling fan was used and was placed opposite the light flow. The reported emission spectra in Fig. 24.

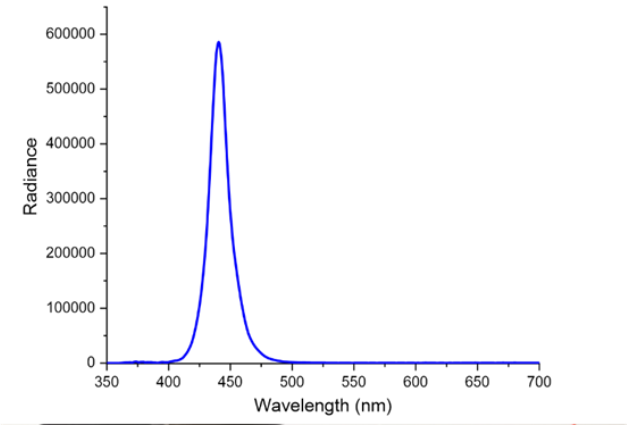

Figure 24: Emission spectra of the lamp

8.3 1H-NMR ANALYSIS OF REAGENTS, PRODUCT AND SIDE PRODUCTS

The concentrations of the compounds were collected using the 1H-NMR analysis by the Varian 400 spectrometer. In the Figure below there are the stoichiometric compounds involved in the reactions, with the respective signals in the NMR spectra (Figure 25). In the order, there are 4-methyl-iodobenzoate (**1**) or 4-methyl-bromobenzoate (**10**), the (*tert*-butoxycarbonyl)proline (**2**), the methyl benzoate (**13**), the 4-hydroxybenzoate (**14**), the 1-(*tert*-butyl) 2-(4-(methoxycarbonyl)phenyl) pyrrolidine-1,2-dicarboxylate (**3**) and the 1,3,5-trimethoxybenzene (**15**) (Figure 25) with the reported NMR spectra (Figure 26).

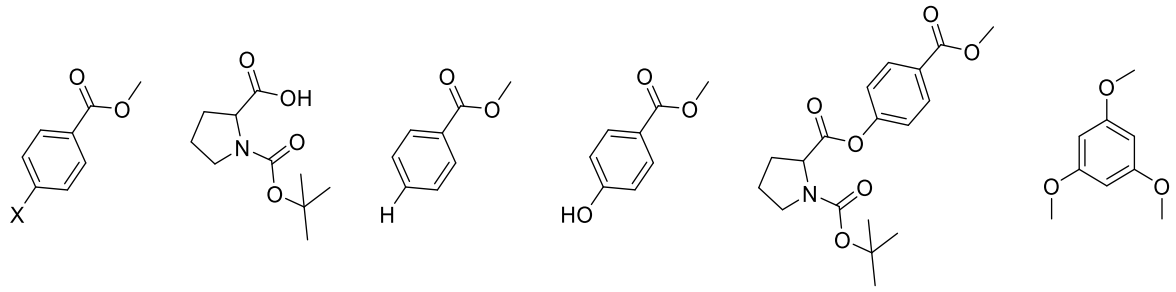

Figure 25: The main compounds analyzed in the NMR spectra

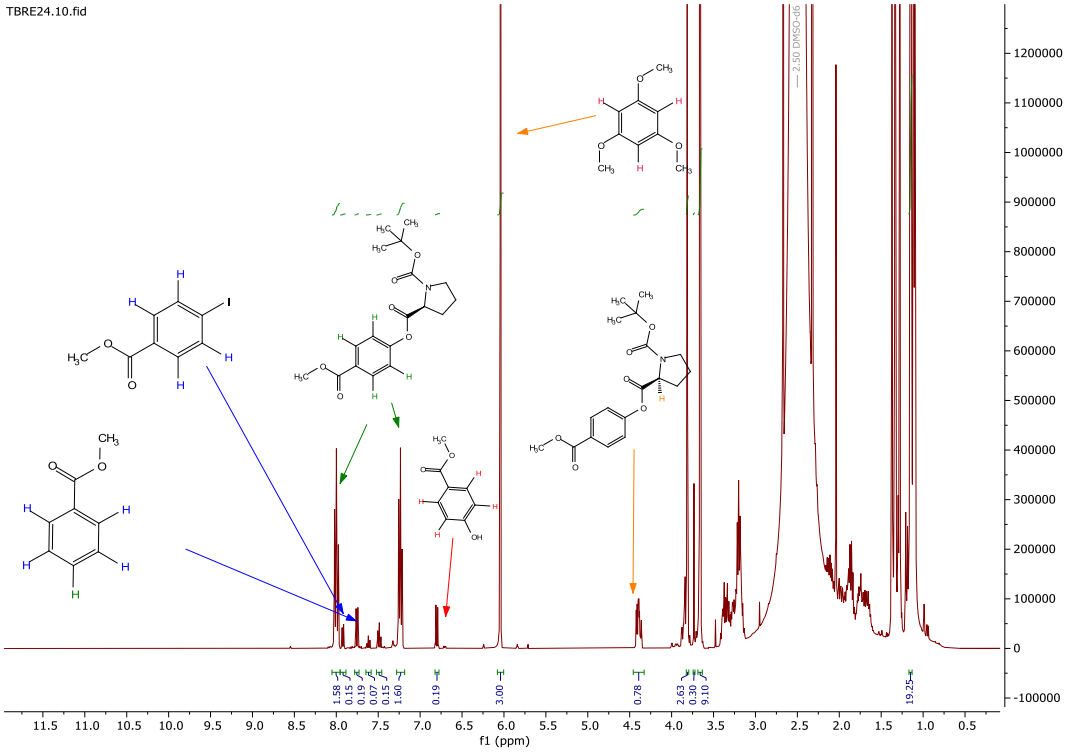

Figure 26 1H-NMR spectra for collecting final concentrations

8.4 TECHNIQUE VALIDATION PROCEDURE

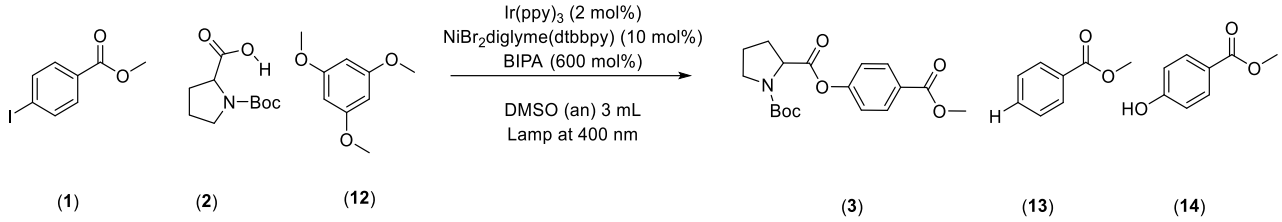

Figure 27 Reaction scheme for the technique validation

The experiment (Figure 27) was conducted following the general procedure described. Compound (**12**) (100 mM) was added to the reaction mixture as an internal standard. Periodically, small aliquots (~50 µL) of the reaction solution were taken and subjected to 1H-NMR analysis. Sampling of aliquots for ex situ NMRs initiated upon light irradiation of the reaction mixture and the time intervals were noted. Referring to the final NMR yield, ReactIR yields were calculated from the raw absorbance data, which was scaled and normalised. Given the overlap between the two independent data sets, shown below, ReactIR was found to be an appropriate measure for the progress of the reaction.

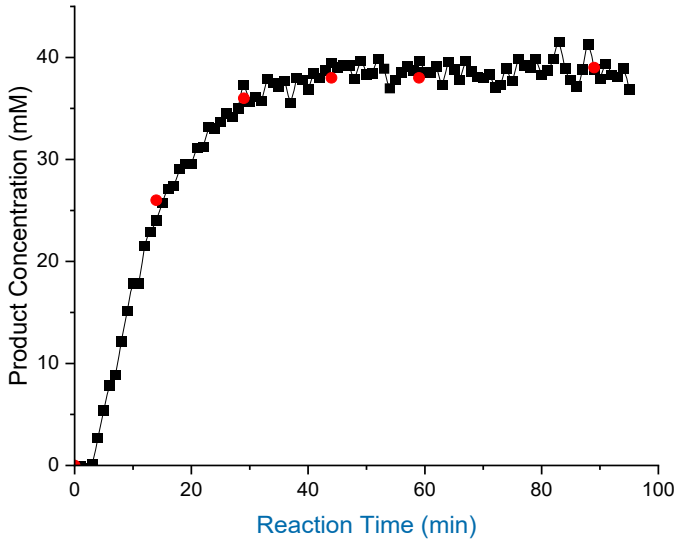

Time [min]	Yield [%]	ReactIR Yield [%]	Difference Yield [%]
0	0	1.5	1.5
15	53	48	4.4
30	72	75	2.6
45	79	75	3.9
60	79	75	4.2
90	78	78	0.2

8.5 PREPARATION OF GRAPHITIC CARBON NITRIDE (g-CN-OA-m)

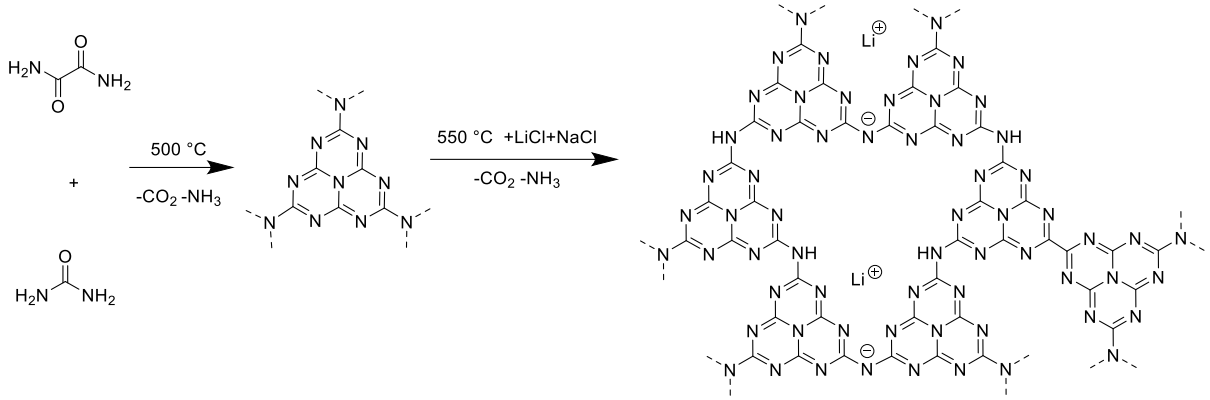

Figure 28 Reaction scheme of the preparation of graphitic carbon nitride (g-CN-OA-m)

Graphitic carbon nitride was prepared according to the procedure described in literature.[45]

Each batch of photocatalyst graphitic carbon nitride was prepared from oxamide (5.7 mmol, 0.5 g), urea (166.5 mmol, 10 g), mixed with Distilled water (10 mL) and stirred for 12 hours at rt. The reaction mixture was dried at 100 °C, the resulting white solids were ground and transferred into a cruicible with a cover. The powder was placed in an air oven and calcinated at 500 °C (v = 4.3 K/min) for 2 hours, obtaining the carbon nitride as a yellow crusty solid. The solid was ground with potassium chloride (44.3 mmol, 3.3 g) and lithium chloride (63.7 mmol, 2.7 mg). The mixtures were heated in a nitrogen fluxed oven at 550 °C (v = 4.6 K/min) for 2 h. The solids obtained were ground and washed with DI water. The resulting powder was dried at 100 °C. The resulting yellow powder (average yield ~400 mg/batch) was analyzed via UV/VIS spectroscopy (Figure 29). 496 mg of this powder was obtained during the procedure.

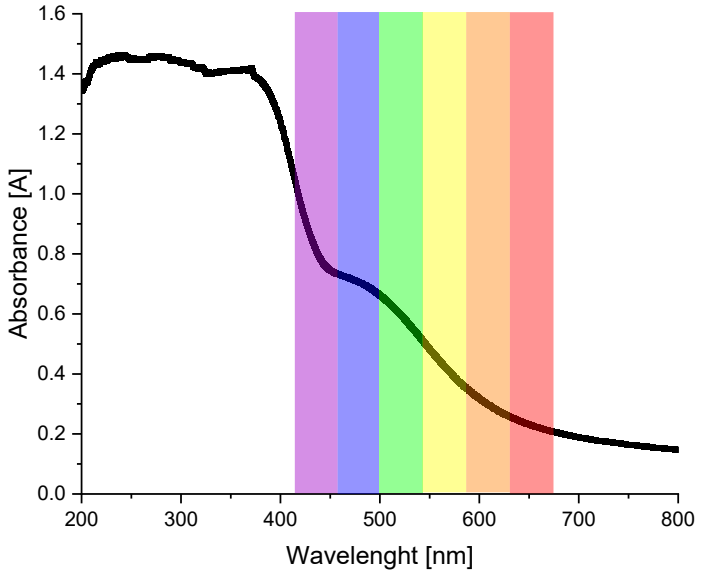

Figure 29: Absorption spectra of g-CN-OA-m

8.6 SYNTHESIS OF *N*-isopropyl-2-methylpropan-2-amine

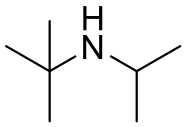

N-isopropyl-2-methylpropan-2-amine was prepared according to the procedure described by literature.[46] A round bottom flask *tert*-butylamine (131.7 g, 189.2 mL, 1.8 mol), isopropyl bromide (147.6 g, 112.7 mL, 1.2 mol), tetrabutylammonium iodide (44.3 g, 0.1 mol) and adiponitrile (136.49 mL) were added and heated to 60 °C for 18 h. After 18 hours the temperature was increased to 75 °C for 48 h. The reaction mixture was left to cool to room temperature and washed with 400 mL of NaOH (5 M). The mixture was extracted with 500 mL of pentane, saving the higher of the three layers obtained. The pentane phase was distilled by fractional distillation, followed by the desired amine at 98 °C. The amine was isolated as a colourless liquid (74.1 mg, 53.7%).

^{1}H NMR (400 MHz, $CDCl_3$) δ 0.98 (d, *J* = 4 Hz, 6 H), δ 1.03 (s, 9 H), δ 2.86 (m, 1 H). (Figure 30)

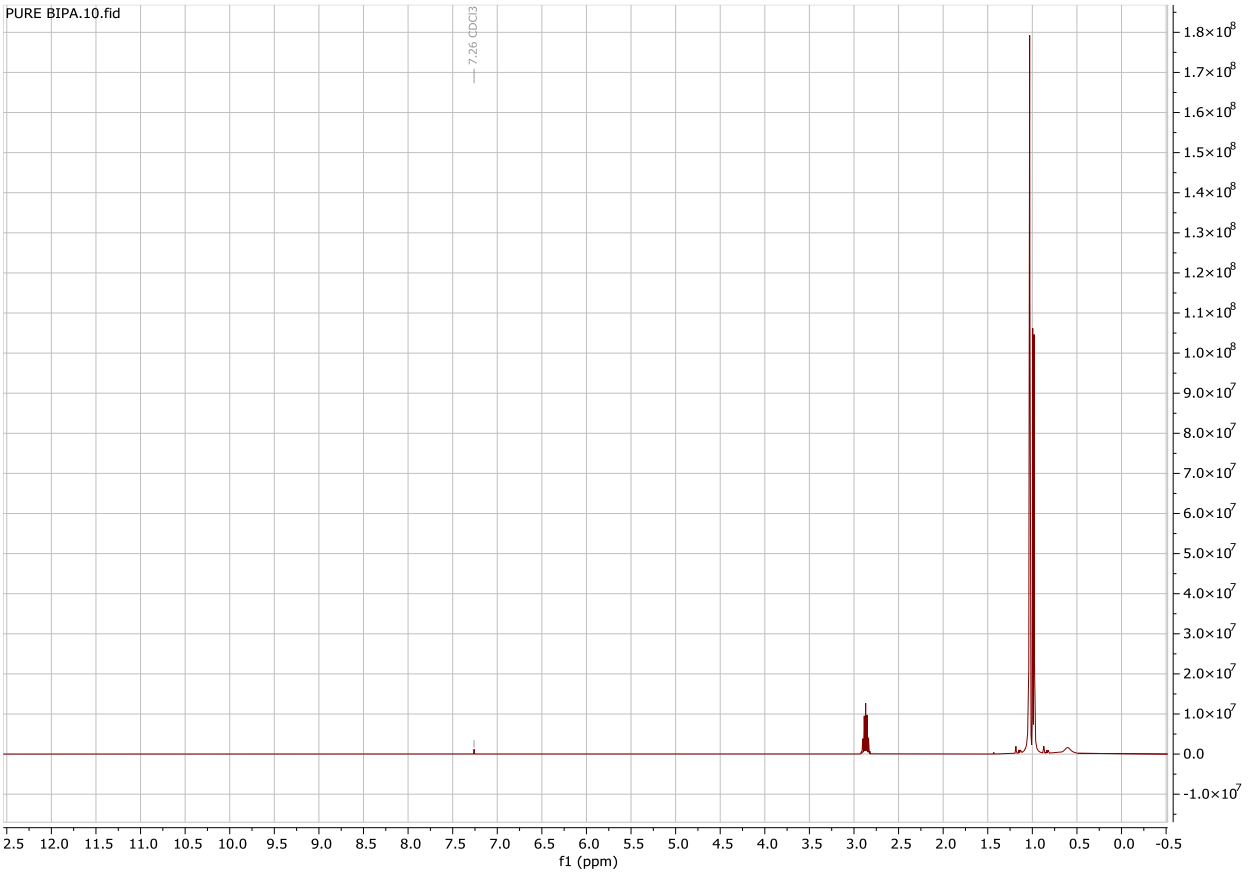

Figure 30 1H-NMR of distilled of N-isopropyl-2-methylpropan-2-amine

8.7 SAME EXCESS EXPERIMENT

Following the general procedure outlined above (2.1.2), two experiments were conducted with the same excess procedure. A difference of molarity (50 mM) was maintained constant between the reagent (**1**) and the reagent (**2**) in each reaction.

8.7.1 INVESTIGATION OF THE SYSTEM $Ir(ppy)_3$ –Nickel(II) WITH Ar-I

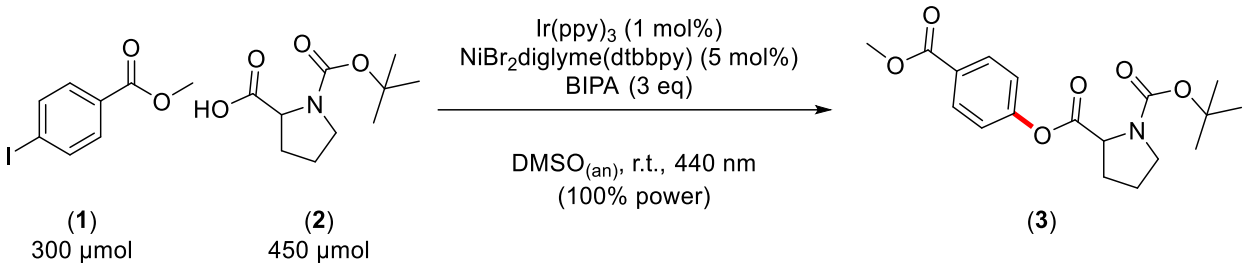

(**1**) 300 µmol (**2**) 450 µmol (**3**)

Reaction	(1) [%] final	(3) [%]	(13) [%]	(14) [%]	Total [%]
Entry 1	4	89	3	2	98

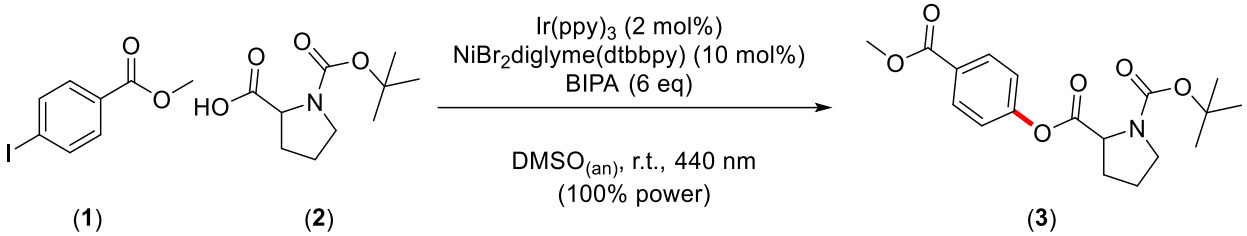

(**1**) 150 µmol (**2**) 300 µmol (**3**)

Reaction	(1) [%] final	(3) [%]	(13) [%]	(14) [%]	Total [%]
Entry 2	6	84	3	4	97

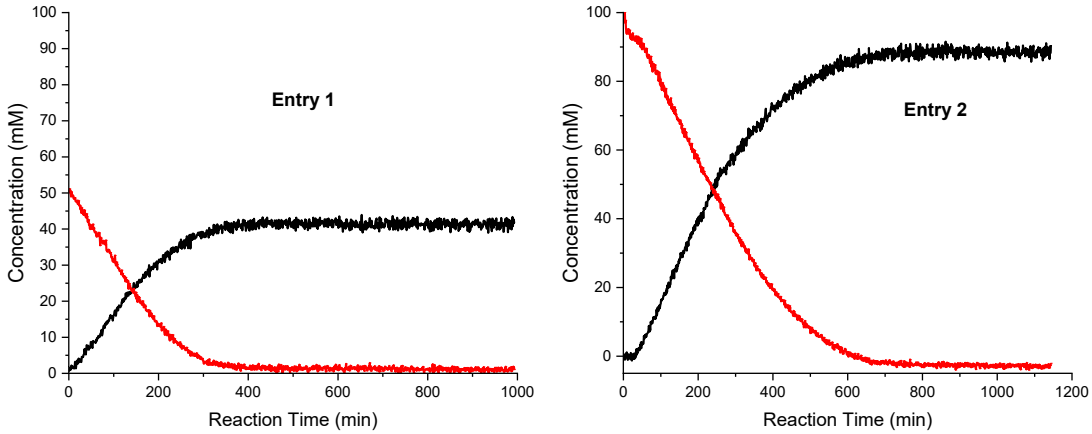

8.7.2 INVESTIGATION OF THE SYSTEM $Ir(ppy)_3$ –Nickel(II) WITH Ar-Br

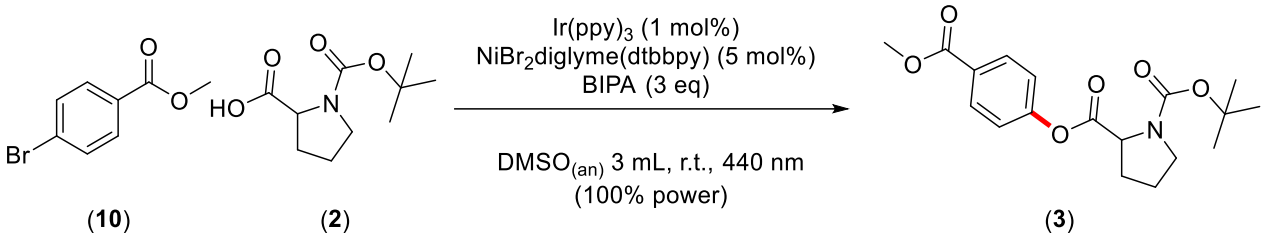

(**10**) 300 µmol (**2**) 450 µmol (**3**)

Reaction	(10) [%] final	(3) [%]	(13) [%]	(14) [%]	Total [%]
Entry 1	14	79	11	2	106

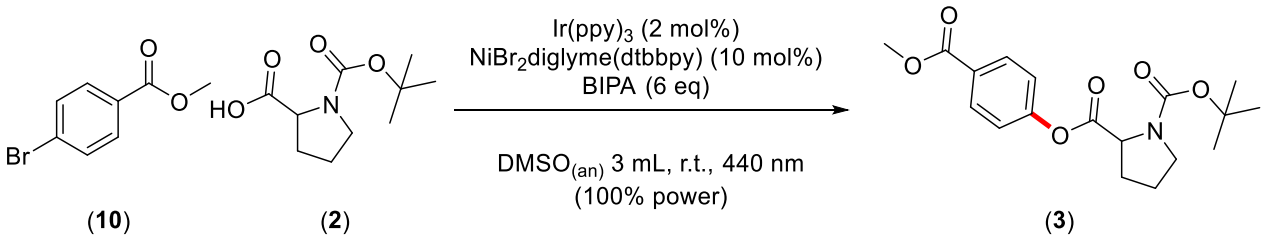

(**10**) 150 µmol (**2**) 300 µmol (**3**)

Reaction	(10) [%] final	(3) [%]	(13) [%]	(14) [%]	Total [%]
Entry 2	16	74	14	2	106

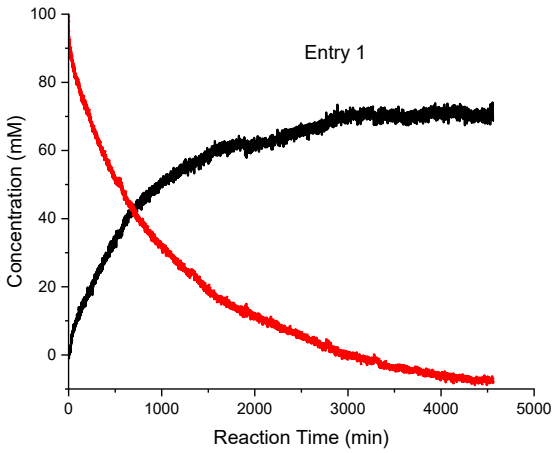

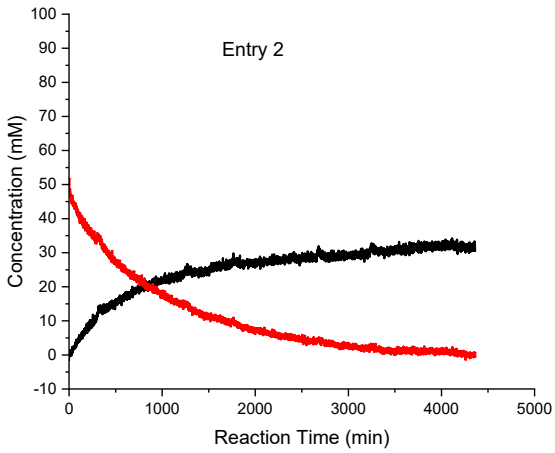

8.7.3 INVESTIGATION OF THE SYSTEM g-CN-OA-m – Nickel(II) WITH Ar-I

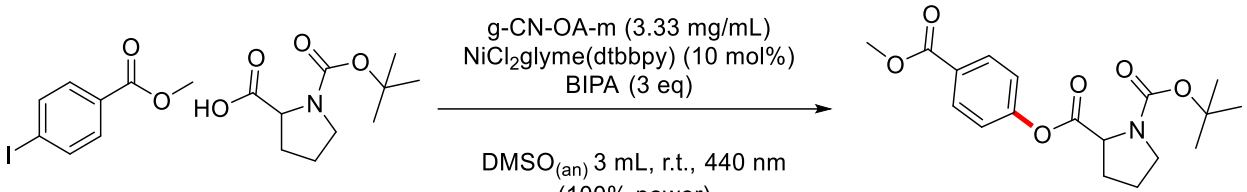

(**1**) 300 µmol (**2**) 450 µmol (**3**)

Reaction	(1) [%] final	(3) [%]	(13) [%]	(14) [%]	Total [%]
Entry 1	8	78	7	10	103

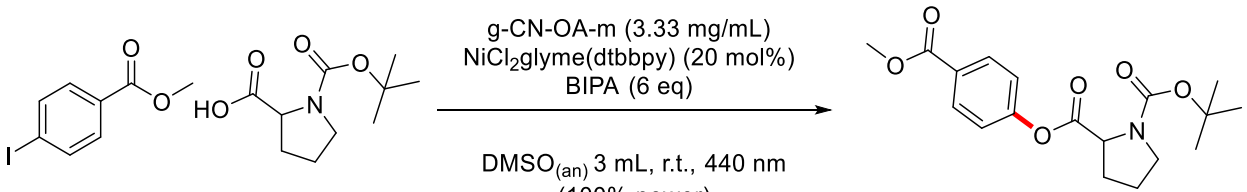

(**1**) 150 µmol (**2**) 300 µmol (**3**)

Reaction	(1) [%] final	(3) [%]	(13) [%]	(14) [%]	Total [%]
Entry 2	4	89	4	2	99

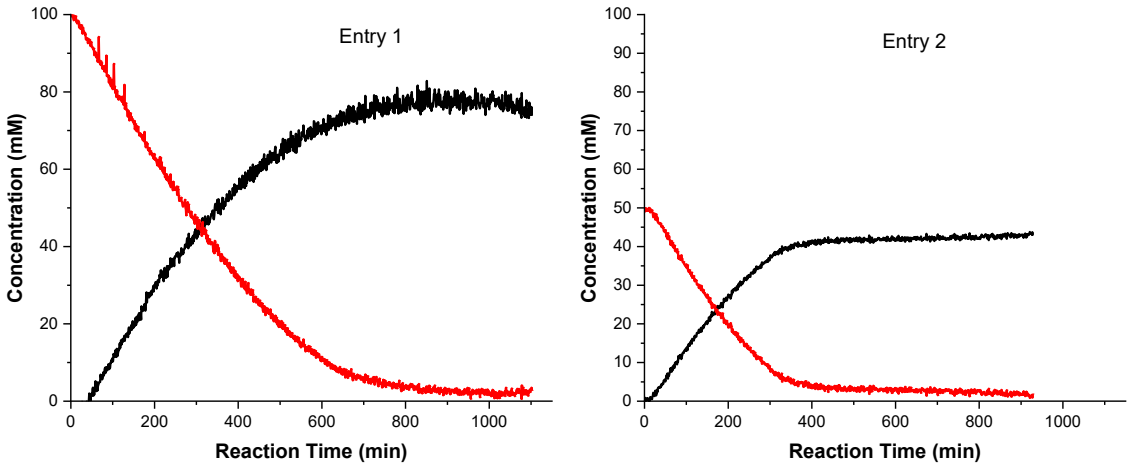

8.7.4 INVESTIGATION OF THE SYSTEM g-CN-OA-m – Nickel(II) WITH Ar-Br

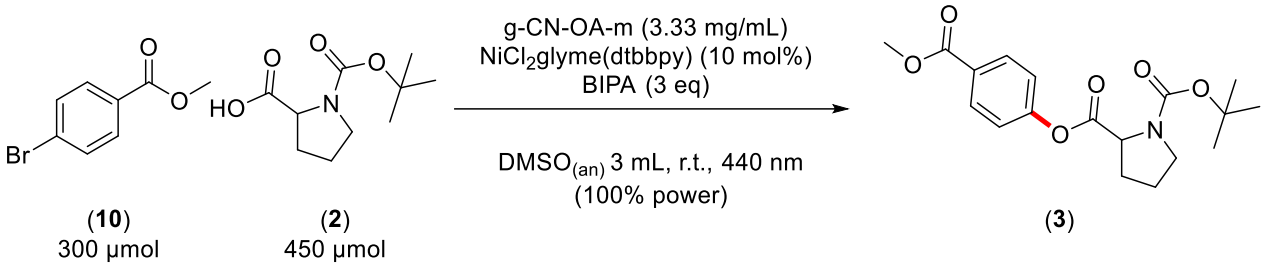

(**10**) 300 µmol (**2**) 450 µmol (**3**)

Reaction	(10) [%] final	(3) [%]	(13) [%]	(14) [%]	Total [%]
Entry 1	4	89	3	2	98

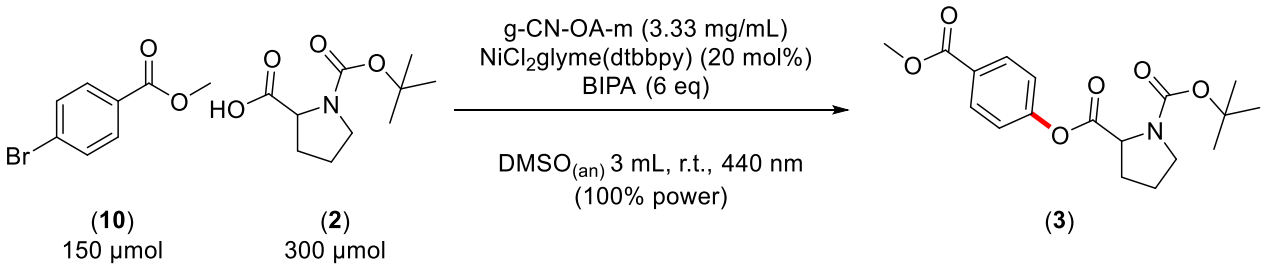

(**10**) 150 µmol (**2**) 300 µmol (**3**)

Reaction	(10) [%] final	(3) [%]	(13) [%]	(14) [%]	Total [%]
Entry 2	6	84	6	2	98

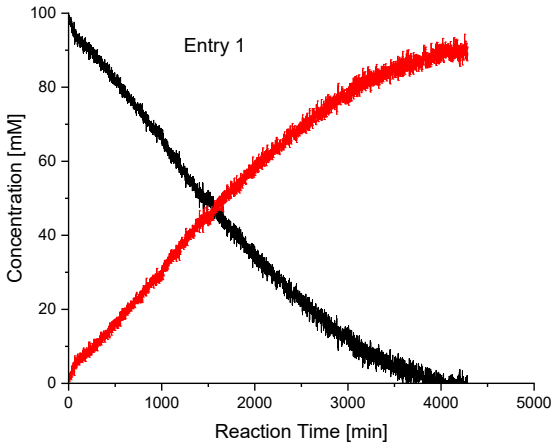

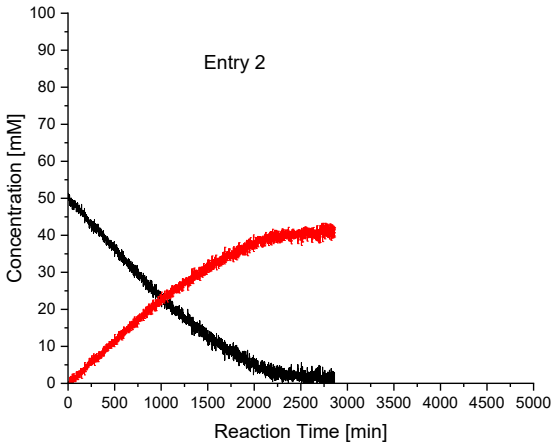

8.7.5 INVESTIGATION OF THE SYSTEM Ni(II)-czbpy WITH Ar-I

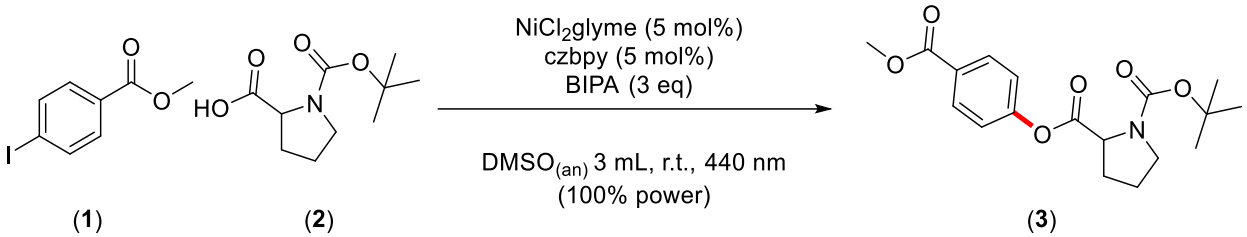

(**1**) 300 µmol (**2**) 450 µmol (**3**)

Reaction	(1) [%] final	(3) [%]	(13) [%]	(14) [%]	Total [%]
Entry 1	5	80	5	5	95

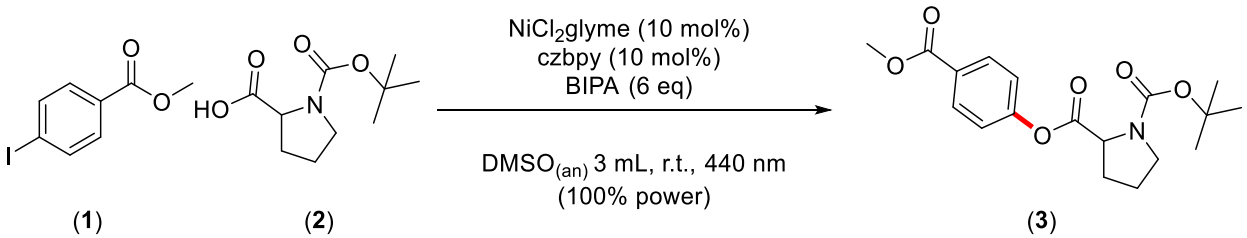

(**1**) 150 µmol (**2**) 300 µmol (**3**)

Reaction	(1) [%] final	(3) [%]	(13) [%]	(14) [%]	Total [%]
Entry 2	6	76	6	6	94

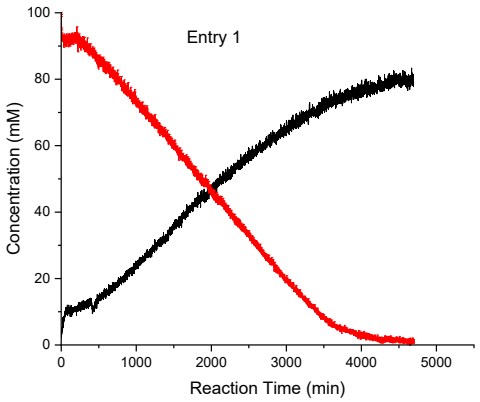

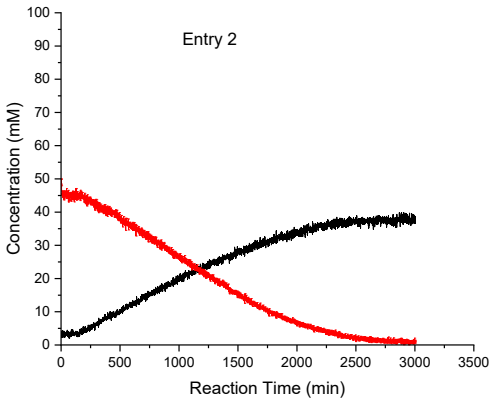

8.7.6 INVESTIGATION OF THE SYSTEM poly-Ni(II)-czbpy WITH Ar-I

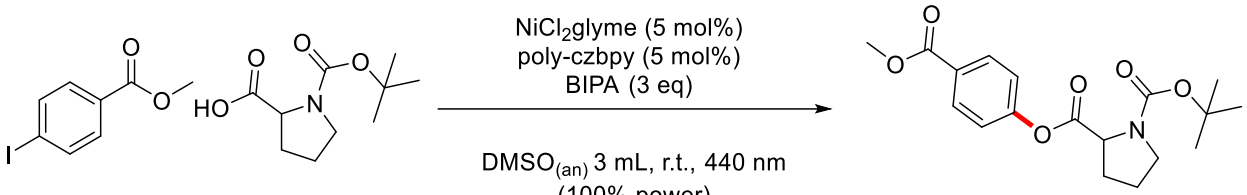

(**1**) 300 µmol (**2**) 450 µmol (**3**)

Reaction	(1) [%] final	(3) [%]	(13) [%]	(14) [%]	Total [%]
Entry 1	26	49	14	4	93

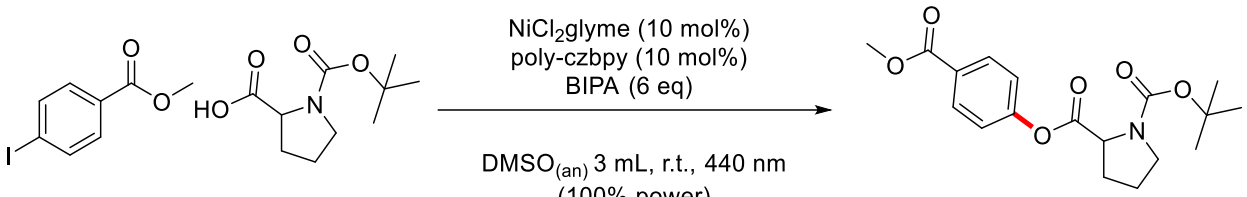

(**1**) 150 µmol (**2**) 300 µmol (**3**)

Reaction	(1) [%] final	(3) [%]	(13) [%]	(14) [%]	Total [%]
Entry 2	28	52	16	4	100

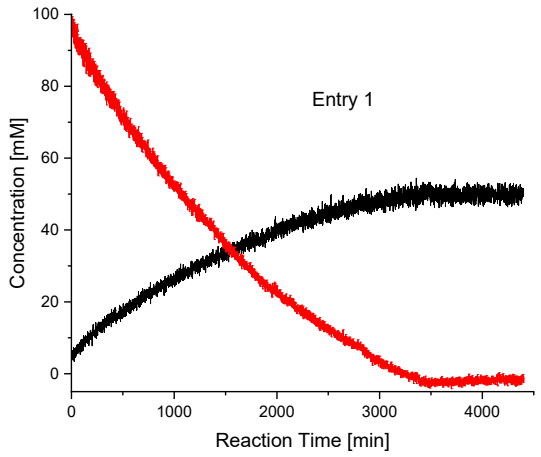

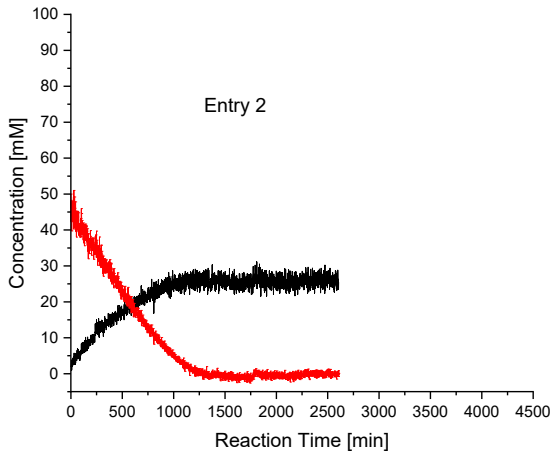

8.7.6.1 PROOVING REACTION FOR INVESTIGATION OF THE SYSTEM poly-Ni(II)-czbpy WITH Ar-I

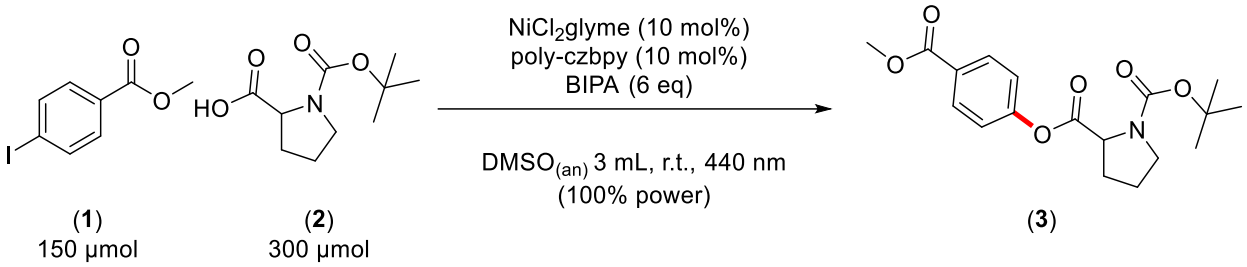

The Entry 1 was prepared in an oven dried round bottom flask of 1 mL. It was loaded with a magnetic stir bar, N-Boc proline (2) (17.69 mg, 82.21 µmol), 4-methyl-iodobenzoate (1) (10.77 mg, 41.10 µmol), the poly-5,5'-di(9H-carbazol-9-yl)-2,2'-bipyridine (2 mg, 0.53 µmol), the Nickel(II) chloride ethylene glycol dimethyl ether complex (0.9 mg, 0.53 µmol), the DMSO (3 mL) and *N*-isopropyl-2-methylpropan-2-amine (39.1 µL, 0.246 µmol).

The Entry 2 was prepared in the same condition of the Entry 2, also with the 1-(*tert*-butyl) 2-(4-(methoxycarbonyl)phenyl) pyrrolidine-1,2-dicarboxylate (**3**) (14.35 mg, 41.10 µmol).

ABBREVIATIONS

Ar-Br	4-methyl-bromobenzoate
Ar-I	4-methyl-iodobenzoate
BIPA	*N*-isopropyl-2-methylpropan-2-amine
czbpy	5,5'-Di(9*H*-carbazol-9-yl)-2,2'-bipyridine
Diglyme	diethylene glycol dimethyl ether complex
$DMSO_{(an)}$	Dimethylsulfoxide anhydrous
dtbbpy	4,4'-di-*tert*-butyl-2,2'-bipyridyl
EnT	Energy Transfer
FTIR	Fourier Transform Infrared Spectroscopy
g-CN-OA-m	Graphitic carbon nitride
glyme	1,2-Dimethoxyethane
ISC	Inter-system-crossing
MLCT	Metal-to-Ligand charge transfer
N-Boc-Prol	N-Boc-L-proline
PC	Photocatalyst
PC*	Excited Photocatalyst
poly-czbpy	Poly-5,5'-Di(9H-carbazol-9-yl)-2,2'-bipyridine
ppy	2-phenylpyridine
Prod	1-(*tert*-butyl) 2-(4-(methoxycarbonyl)phenyl) pyrrolidine-1,2-dicarboxylate
r.t.	Room temperature
SCE	Satured calomel electrode
SET	Single electron transfer

DECLARATION OF AUTHENTICITY

I herewith declare that I wrote this thesis on my own and did not use any unnamed sources or aid. Thus, to the best of my knowledge and belief, this thesis contains no material previously published or written by another person except where due reference is made by correct citation. This includes any thoughts taken over directly or indirectly from printed books and articles as well as all kinds of online material. It also includes my own translations from sources in a different language.
The work contained in this thesis has not been previously submitted for examination.
I also agree that the thesis may be tested for plagiarized content with the help of plagiarism software. I am aware that failure to comply with the rules of good scientific practice has grave consequences and may result in expulsion from the programme.

REFERENCES

1. Sperry, J. B.; Price Wiglesworth, K. E.; Edmonds, I.; Fiore, P.; Boyles, D. C.; Damon, D. B.; Dorow, R. L.; Piatnitski Chekler, E. L.; Langille, J.; Coe, J. W., *Organic Process Research & Development* **2014,** 18 (12), 1752-1758.

2. Devendar, P.; Qu, R.-Y.; Kang, W.-M.; He, B.; Yang, G.-F., *Journal of Agricultural and Food Chemistry* **2018,** 66 (34), 8914-8934.

3. Ruiz-Castillo, P.; Buchwald, S. L., *Chemical Reviews* **2016,** 116 (19), 12564-12649.

4. Lyons, T. W.; Hull, K. L.; Sanford, M. S., *Journal of the American Chemical Society* **2011,** 133 (12), 4455-4464.

5. Zhu, C.; Yue, H.; Jia, J.; Rueping, M., *Angewandte Chemie International Edition* **2021,** 60 (33), 17810-17831.

6. Chernyshev, V. M.; Ananikov, V. P., *ACS Catalysis* **2022,** 12 (2), 1180-1200.

7. Hartwig, J. F., *Accounts of Chemical Research* **1998,** 31 (12), 852-860.

8. Welin, E. R.; Le, C.; Arias-Rotondo, D. M.; McCusker, J. K.; MacMillan, D. W., *Science* **2017,** 355 (6323), 380-385.

9. Chen Zhu†, H. Y., Pavlo Nikolaienko and Magnus Rueping, *CCS Chemistry* **2020,** 2 (2), 179-190.

10. Marzo, L.; Pagire, S. K.; Reiser, O.; König, B., *Angewandte Chemie International Edition* **2018,** 57 (32), 10034-10072.

11. Keane, D. A.; McGuigan, K. G.; Ibáñez, P. F.; Polo-López, M. I.; Byrne, J. A.; Dunlop, P. S. M.; O'Shea, K.; Dionysiou, D. D.; Pillai, S. C., *Catalysis Science & Technology* **2014,** 4 (5), 1211-1226.

12. Osterloh, F. E., *ACS Energy Lett.* **2017,** 2, 445.

13. Jespersen, J. E. B. F. A. S. N. D., *Chemistry: International Student Version*

Fifth Edition ed.; John Wiley & Sons, Inc: 2009; Vol. 1, p 548-557.

14. Zuo, Z.; Ahneman, D. T.; Chu, L.; Terrett, J. A.; Doyle, A. G.; MacMillan, D. W. C., *Science* **2014,** 345, 437.

15. Sun, R.; Qin, Y.; Ruccolo, S.; Schnedermann, C.; Costentin, C.; Nocera, D. G., *Journal of the American Chemical Society* **2019,** 141 (1), 89-93.

16. Emily B. Corcoran, M. T. P., Shishi Lin, Spencer D. Dreher, Daniel A. DiRocco, Ian W. Davies, Stephen L. Buchwald and David W. C. MacMillan, *Science* **2016,** 353 (6296), 279-283.

17. Braslavsky, S. E., *Pure and Applied Chemistry* **2007,** 79 (3), 293-465.

18. Arias-Rotondo, D. M.; McCusker, J. K., *Chemical Society Reviews* **2016,** 45 (21), 5803-5820.

19. Djurišić, A. B.; He, Y.; Ng, A. M. C.; X., L. J.; G., Y. J.; M., J.; S., W.; A., A.-G. A., *APL Materials* **2020,** 8 (3), 030903.

20. Pieber, B.; Malik, J. A.; Cavedon, C.; Gisbertz, S.; Savateev, A.; Cruz, D.; Heil, T.; Zhang, G.; Seeberger, P. H., *Angewandte Chemie International Edition* **2019,** 58 (28), 9575-9580.

21. Cavedon, C.; Madani, A.; Seeberger, P. H.; Pieber, B., *Organic Letters* **2019,** 21 (13), 5331-5334.

22. Reischauer, S.; Strauss, V.; Pieber, B., *ACS Catalysis* **2020,** 10 (22), 13269-13274.

23. Zhao, Z.; Reischauer, S.; Pieber, B.; Delbianco, M., *Green Chemistry* **2021,** 23 (12), 4524-4530.

24. Cristian Cavedon, S. G., Sarah Vogl, Noah Richter, Stefanie Schrottke,; Christian Teutloff, P. H. S., Arne Thomas and Bartholomäus Pieber. Photocatalyst-free, visible-light-mediated nickel catalyzed

carbon–heteroatom cross-couplings *Cambridge Open Engage* [Online], 2021, p. 1-15.

25. Kawamata, Y.; Vantourout, J. C.; Hickey, D. P.; Bai, P.; Chen, L.; Hou, Q.; Qiao, W.; Barman, K.; Edwards, M. A.; Garrido-Castro, A. F.; deGruyter, J. N.; Nakamura, H.; Knouse, K.; Qin, C.; Clay, K. J.; Bao, D.; Li, C.; Starr, J. T.; Garcia-Irizarry, C.; Sach, N.; White, H. S.; Neurock, M.; Minteer, S. D.; Baran, P. S., *Journal of the American Chemical Society* **2019,** 141 (15), 6392-6402.

26. Gisbertz, S.; Reischauer, S.; Pieber, B., *Nature Catalysis* **2020,** 3 (8), 611-620.
27. J., A. P. d. P., *Atkins' Physical Chemistry*. 8th ed.; 2006; Vol. 1.
28. Blackmond, D. G., *Angewandte Chemie International Edition* **2005,** 44 (28), 4302-4320.
29. Blackmond, D. G.; Ropic, M.; Stefinovic, M., *Organic Process Research & Development* **2006,** 10 (3), 457-463.
30. Nielsen, C. D. T.; Burés, J., *Chemical Science* **2019,** 10 (2), 348-353.
31. Marcus, R. A., *Angewandte Chemie International Edition in English* **1993,** 32 (8), 1111-1121.
32. de Oliveira, G. X.; Lira, J. O. d. B.; Riella, H. G.; Soares, C.; Padoin, N., *Frontiers in Chemical Engineering* **2022,** 3.
33. Terrett, J. A.; Cuthbertson, J. D.; Shurtleff, V. W.; MacMillan, D. W. C., *Nature* **2015,** 524 (7565), 330-334.
34. Malik, J. A.; Madani, A.; Pieber, B.; Seeberger, P. H., *Journal of the American Chemical Society* **2020,** 142 (25), 11042-11049.
35. Markushyna, Y.; Smith, C. A.; Savateev, A., *European Journal of Organic Chemistry* **2020,** 2020 (10), 1294-1309.
36. Zhang, G.; Li, G.; Lan, Z.-A.; Lin, L.; Savateev, A.; Heil, T.; Zafeiratos, S.; Wang, X.; Antonietti, M., *Angewandte Chemie International Edition* **2017,** 56 (43), 13445-13449.
37. Savateev, A.; Ghosh, I.; König, B.; Antonietti, M., *Angewandte Chemie International Edition* **2018,** 57 (49), 15936-15947.
38. Luis Arnaut, S. F. a. H. B., *Chemical Kinetics From Molecular Structure to Chemical Reactivity*. Elsevier Science: 2006.
39. Sahoo, H., *Journal of Photochemistry and Photobiology C-photochemistry Reviews* **2011,** 12, 20-30.
40. Dexter, D. L., *The Journal of Chemical Physics* **1953,** 21 (5), 836-850.
41. Pein, B. C.; Seong, N.-H.; Dlott, D. D., *The Journal of Physical Chemistry A* **2010,** 114 (39), 10500-10507.
42. Borah, J. M.; Chowdhury, P., *Steroids* **2011,** 76 (12), 1341-1345.
43. Li, Y.; Zou, Y., *Advanced Materials* **2008,** 20 (15), 2952-2958.
44. J., A. P. d. P., *Atkins' Physical Chemistry*. 9th ed.; OUP Oxford: 2009; p 13.
45. Savateev, A.; Pronkin, S.; Epping, J. D.; Willinger, M. G.; Antonietti, M.; Dontsova, D., *Journal of Materials Chemistry A* **2017,** 5 (18), 8394-8401.
46. Evans, V.; Mahon, M. F.; Webster, R. L., *Tetrahedron* **2014,** 70 (41), 7593-7597.

RINGRAZIAMENTI

Vorrei ringraziare I miei genitori, mia sorella e il resto della mia famiglia, che in questi anni universitari mi sono stati di supporto, sia finanziariamente che economicamente.

I would like to thank Bart and his group, especially Amiera, for the special opportunity they gave to me, to visit their research lab and especially for the time they spent to help me.

Ringrazio tutti i miei amici di lunga e corta data, in particolare Marlene, senza la quale non avrei mai avuto l'idea di effettuare un tirocinio all'estero e durante il quale mi ha anche aiutato.

Ringrazio inoltre il professor Formaggio, il quale mi ha aiutato molto in questo ultimo periodo con la tesi.

Infine ringrazio tutti voi che avete dedicato un po' del vostro tempo per leggere la mia tesi.